CHEMICAL REVIEWS

Review

pubs.acs.org/CR

Tip-Enhanced Raman Spectroscopy: Technique and Recent Advances

Prabhat Verma*

Department of Applied Physics, Osaka University, 2-1 Yamadaoka, Suita, Osaka 565-0871, Japan

ABSTRACT: This review discusses a relatively new technique for optical nanoimaging at visible wavelength, known as tip-enhanced Raman spectroscopy (TERS). This technique relies on the enhancement and spatial confinement of light in the close vicinity of the apex of a plasmonic nanotip. The plasmonic nanotip can be positioned on the sample and controlled by a suitable scanning probe microscopy, such as atomic force microscopy or scanning tunneling microscopy. By raster scanning the nanotip, one can obtain nanoimages with high spatial resolution. While enhancement helps measuring weak phonon modes from a tiny volume of the sample, confinement delivers extremely high spatial resolution in nanoimaging. We will discuss the technique of TERS in more detail with several applications and review the recent advances.

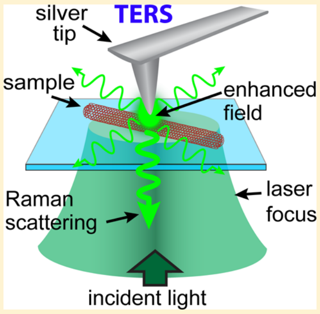

CONTENTS

1. INTRODUCTION

This review discusses the technique of tip-enhanced Raman spectroscopy (TERS), which combines Raman spectroscopy with scattering (or apertureless) scanning near-field optical microscopy (s-SNOM) to realize Raman spectroscopy and Raman imaging at the nanoscale, far beyond the diffraction limit of the probing light. It utilizes the local mode of surface plasmons of a sharp metallic nanotip to confine and enhance the light field in the vicinity of the tip apex, which can be used to excite Raman scattering from a nanoscopic volume of a sample placed under the tip. By scanning the tip on the sample surface, one can obtain a Raman image of the sample with a nanometric spatial resolution. Therefore, TERS allows one to optically analyze and image a sample with extremely high spatial resolution. The technique of TERS has matured over the years, improved spatial resolutions have been demonstrated, and new applications have been proposed. Particularly, TERS imaging in the recent past has shown vital insight into the spatial distribution of chemicals, biomolecules, and physical or electronics properties on the surface of a sample at a spatial resolution that was unachievable by any other optical or analytical methods. The motivation of this review is to revisit the development of this technique and to encourage its further applications in nanoanalyzing and nanoimaging various samples ranging from materials to biomolecules.

2. BRIEF HISTORY

In most research fields of physics, chemistry, and biology, it is of fundamental importance to characterize the physical properties of the sample, the surface adsorbates and the molecular distributions, and the bioactivities at the nanoscale

Received: December 9, 2016
Published: May 1, 2017

DOI: 10.1021/acs.chemrev.6b00821
Chem. Rev. 2017, 117, 6447−6466

through an accurate and nondestructive technique. Optical techniques, such as vibrational spectroscopy or optical microscopy, are often adopted to nondestructively study the intrinsic properties of a sample. Indeed, vibrational spectroscopy is a very powerful tool, because it can potentially show vibrational modes of every single molecule present in the sample and, thus, accurately reflects the chemical content of the sample. For this reason, vibrational spectroscopy is widely used in chemical and biological studies where one wants to obtain the accurate chemical information on a sample. On the other hand, optical microscopy, particularly combined with scanning techniques, provides a mapping of the sample on a wider area. When one combines spectroscopy with microscopy, a technique termed as spectro-microscopy, it is possible to obtain the chemical distribution over a large area of a sample. In a typical spectro-microscopic technique, the sample is raster scanned and vibrational scattering is measured from each point of the sample during the scanning. This means that each pixel in the scanned image contains full vibrational spectroscopic information on the sample at that particular point from where the image pixel was obtained. This tremendously strengthens the information content of the image, because one can select any particular vibrational mode in each pixel and construct an image that shows the spatial distribution of that particular molecule of the sample that is associated with the selected vibrational mode. In this way, one can simultaneously construct several images from various vibrational modes and by overlaying these images, one can obtain full chemical distribution over a large area of the sample. Tip-enhanced Raman microscopy, which will be discussed in this review, is one example of the spectro-microscopy at the nanoscale.

Although optical spectroscopy and microscopy techniques are very convenient tools to study the intrinsic properties of a sample with nondestructive approaches, they are usually very weak and have a strong restriction on the spatial resolution that is governed by the diffraction limit of light. Specifically, Raman scattering is an extremely weak phenomenon, which becomes even weaker when one talks about samples of nanometer size. This brings in an inherent practical difficulty in utilizing techniques based on Raman scattering to analyze samples at nanoscale. The discovery of surface-enhanced Raman spectroscopy (SERS)[1−3] in 1970s was a milestone in the field of Raman scattering, where researchers demonstrated enhancement of Raman scattering by a factor of 10^{10}−10^{14} and made it possible to measure Raman scattering even from a single molecule. Soon after its discovery, SERS was well recognized and has been intensely studied and widely utilized in many areas.[4−23]

2.1. Surface-Enhanced Raman Spectroscopy

SERS utilizes either roughened metallic surface or clusters of metallic nanoparticles, on which the sample molecules are adsorbed.[24−27] In fact, the nanometric roughness of a metallic surface also acts as metallic nanoparticles placed close to each other. Depending upon the variation in the shape and size of these nanoparticles, the resonance of the localized surface plasmons can have a particular wavelength and spectral width. Therefore, when illuminated with a propagating light of suitable wavelength, the localized surface plasmons can be resonantly excited to produce a strongly enhanced evanescent or near-field light in the vicinity of these nanoparticles, where the sample molecules are adsorbed. The strongly enhanced light produces enhanced Raman scattering from the adsorbed sample molecules. Since Raman scattering takes place in the near-field, the Raman scattered light is also a near-field light, which is converted back to the far-field by the same nanoparticles and is measured by regular Raman measurement systems in the far-field. If the plasmon resonance is broad enough to cover both the incident and the Raman scattered wavelengths, both incident and scattered light can be simultaneously enhanced, delivering much larger enhancement to the measured signal in comparison to the case when the plasmon resonance is narrow and only one out of the two, either incoming or outgoing signal, is enhanced. This mechanism of field enhancement in SERS is usually known as the electromagnetic (EM) or the plasmonic enhancement,[4−6] which is the primary mechanism of enhancement and is argued to produce a massive enhancement factor of about 10^8−10^{11}. A good review on plasmonic enhancement can be found in ref 28. The enhancement in SERS is also enriched by another process known as the chemical enhancement, usually interpreted by the charge-transfer (CT) mechanism,[7,8,13] which contributes to the enhancement by a factor of about 10^2−10^3. However, some studies have indicated that under certain conditions, the chemical enhancement can be much larger than what many researchers have thought.[29−32] Although the enhancement mechanism of SERS has always remained under debate, it is believed that CT is not the only factor that contributes to the chemical enhancement. There are two more mechanisms that contribute to the chemical enhancement in SERS, which arise from the chemical interactions between the adsorbate and the metal nanoparticle. One is the enhancement due to the ground state chemical interactions between the adsorbate molecule and the metal atoms that are not associated with any excitation. The other is due to the resonance Raman effect when the excitation wavelength is in resonance with one of the molecular transitions. Thus, under certain conditions, the chemical enhancement can be much larger, resulting in a huge total enhancement in SERS. A critical review on the enhancement mechanism in SERS can be found in ref 33.

By delivering huge enhancement, SERS provides us an opportunity to overcome the low Raman scattering cross-section of a small number of molecules or nanosized samples, which found wide usage in detecting the vibrational and chemical information from nanosized samples. With such a massive enhancement, SERS can even make it possible to measure Raman scattering from a single molecule, provided the sample molecules are properly spread with low density. For single molecule-SERS (SM-SERS),[10,11] the nanogaps between metallic nanoparticles, also known as the hot spots, play very important roles, because the interaction between the local plasmon modes of the two particles creates a gigantic field enhancement within the gap.[34−36] If a single molecule is placed in such a hot spot, the enormous field enhancement makes it possible to measure Raman scattering from that single molecule. Although many researchers can precisely control the adsorption of sample molecules within a hot spot, they can only do so on a statistical basis.[10−12] The presence of a single molecule in a hot spot is usually confirmed from the distinct temporal fluctuation of SERS intensity caused by the random motion of molecules into and out of the hot spot, which can be averaged out for a larger ensemble of molecules and thus distinguishes a single molecule from a larger ensemble. In the later years, SERS was also demonstrated for the infrared[37,38] and the ultraviolet[39−42] wavelength regions by selecting suitable metals.

While SERS came as a revolutionary addition to Raman spectroscopy due to its ability to immensely enhance the light field, it did not solve the restriction on the spatial resolution in Raman measurement imposed by the diffraction limit of light. Even though SERS is a near-field phenomenon, the enhanced field is confined only in the direction perpendicular to the roughened metallic surface. Since the metallic surfaces used in SERS are typically very large, the lateral confinement of the light is basically restricted to the focus spot, which is at least about half of the wavelength, as commanded by the diffraction limit. Thus, for visible light, the lateral confinement is about 200−400 nm, which is not suitable for the investigation of a sample at the nanoscale. In the case of SM-SERS, one had to make sure, often by means of statistical estimations, that there was only a single sample molecule present within the focus spot to demonstrate the capability of single molecule detection by SERS. One must not confuse between single molecule detection and single molecule resolution. SERS could not provide better spatial resolution than the usual confocal Raman microscopy.

2.2. Issue of Spatial Resolution in Optics

The issue of spatial resolution in optical measurements dates back in history. It arises from the implication of the Heisenberg's uncertainty principle, which is applicable on waves. According to this uncertainty principle, the spatial resolution Δx, which is defined as the minimum distance at which two sources could be unambiguously distinguished in an optical observation, would depend on the uncertainty in the momentum of the light Δk, in such a way that the minimum value of the product $\Delta x \cdot \Delta k$ is nonzero. This condition forces Δx to be a nonzero quantity for any finite value of Δk. The practical value of the spatial resolution therefore depends on both the wavelength of the light, which is related to Δk, and the measurement system used for the observation. Abbe[43] and Rayleigh[44] independently derived the criterion for this spatial resolution in the 19th century. According to Abbe's criterion, Δx can be defined as

$$\Delta x = 0.61\lambda/NA \qquad (1)$$

where the numerical aperture of the optical system, NA, depends on the refractive index of the surrounding medium, n, and on the maximum collection angle of the optical system, θ_{max}, and is defined as $NA = n \sin \theta_{\max}$. For the best practical conditions, the experimental value of Δx turns out to be about half of the wavelength. The diffraction limit imposed by the wave nature of light thus restricts the optical resolution for a visible light to be about 200−400 nm. This is, however, the case of linear measurements, which can be improved a little by nonlinear effects or by saturating the light-matter interaction.

The diffraction limit of light enforces a loss of information at the image plane, because an object much smaller than the wavelength would be imaged in defused shape with a size comparable to the diffraction limit, losing the information on its structural shape. Therefore, a nanosized object cannot be imaged correctly by optical methods. This loss of information in optical imaging of a nanosized object can also be understood by recalling that light is composed of the propagating radiation and the nonpropagating evanescent waves. The evanescent waves cannot exist in the free space and they remain restricted only to the vicinity of their sources. Consequently, if the image is formed at a distant plane, the evanescent component of light cannot participate in image formation, which results in the loss of information at the image plane. In order to avoid this loss, it would be necessary to involve the evanescent part of light in the process of image formation. This essentially means that the process of image formation must be carried out in the close vicinity of the source, including a secondary source such as an optical component or a scattering point. This region of vicinity is often known as the near-field, where the intensity of the evanescent field can be considered significant, usually extending to a few tens of nanometers.

Raman scattering in SERS takes place in the near-field; hence, one would expect high spatial resolution in SERS measurements. However, since the surface area of the SESR substrate is often significantly larger than the wavelength, the evanescent wave extends to a large area in the lateral direction and the resolution is defined by the focal spot. Nevertheless, as one can perhaps guess, if the lateral size of the metallic surface used in SERS is reduced to a few nanometers, one would achieve high spatial resolution in the lateral direction as well, albeit, with a substantial loss in field enhancement due to the reduced volume of the metal.

2.3. Tip-Enhanced Raman Spectroscopy

Realizing the shortcomings of SERS, several researchers attempted to extend this technology in the form of single-point SERS, where, instead of a roughened metallic surface, a metallic nanoparticle was used to enhance the light field. In 1985, Wessel proposed this idea where a single metallic nanoparticle could be controlled by scanning probe microscopy (SPM) technologies for single-point enhancement.[45] In this case, the author proposed that the enhanced light could be three-dimensionally (3D) confined to the vicinity of the metallic nanoparticle, which could be utilized to measure Raman, two-photon, or second-harmonic spectrum from the nanometric volume of a sample placed right under the nanoparticle. A larger surface area of the sample was suggested to be measured by raster scanning the nanoparticle over the surface of the sample. High spatial resolution together with reasonably strong enhancement was hinted. In fact, the idea of utilizing a nanoparticle or a nanoaperture to obtain higher resolution was conceived much earlier in 1928 by Synge,[46] though researchers did not pay much attention on this for a long period. Later in 1994, Kawata's group demonstrated SNOM measurements by optically trapping a single metallic nanoparticle[47] and by raster scanning a metallic nanotip[48] over the surface of a sample. Five years later the same group measured Raman nanospectroscopy through s-SNOM technique using a metallic nanotip that worked as a point enhancer.[49] A year later in 2000, Zenobi, Kawata, Anderson, and Pettinger independently published results on Raman measurements at nanoscale by combining Raman spectroscopy with SPM techniques where metallic nanotips were utilized to enhance and confine the light field.[50−53] Since the light field was enhanced by a tip rather than a surface, Zenobi's group coined the name tip-enhanced Raman spectroscopy (TERS) for this technique. It was demonstrated that TERS can provide a spatial resolution of about 20−30 nm, together with an enhancement factor of about 10^3−10^6, which is much weaker than what was earlier reported for SERS, but still good enough to experimentally measure extremely weak Raman signal that was not observable otherwise. The mechanism of field enhancement in TERS is the same as in SERS, which can be basically considered with two contributions: the electromagnetic enhancement and the chemical enhancement.

However, since the tip in TERS behaves like a single antenna or a point enhancer, it lacks huge gap-mode enhancement due to the multiple hot spots between neighboring nanoparticles, which is the dominating factor of electromagnetic enhancement in SERS. Also, since the sample molecules are often adsorbed on the metal nanoparticles in SERS, which is not the case with TERS, the chemical enhancement in SERS is also larger than that in TERS. Therefore, we often see much larger enhancement in SERS in comparison to TERS. Scanning tunneling microscopy (STM),[54] atomic force microscopy (AFM)[55] and shear force microscopy (SFM) techniques were utilized to position and raster scan the metallic nanotip over a sample surface. TERS was demonstrated with different configurations, which will be discussed later in this review. Figure 1a shows one of the configurations for AFM-based TERS. The tip was prepared by thermal evaporation of silver on a silicon cantilever, a SEM image of which is shown in Figure 1b. By combining Raman spectroscopy with SPM techniques, TERS has the ability to simultaneously measure topography and obtain corresponding spectral information from a sample with nanometric spatial resolution and high sensitivity. It provides a powerful tool for the nanocharacterization of materials. Since its first demonstration in 2000, TERS has attracted a great deal of interest and efforts from researchers working in various fields of physics, chemistry and biosciences. Great results have been published over the years and both sensitivity and spatial resolution of TERS have improved with demonstration of its applications in various fields of science.[56−69]

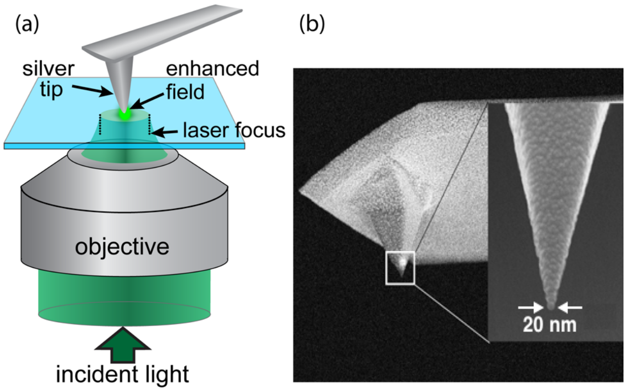

Figure 1. (a) Illustration of an AFM-based TERS measurement system. The incident light is focused on a sample placed on a transparent glass substrate, through a high-NA objective lens. When a silver-coated nanotip is brought in the diffraction-limited focus spot, a strongly enhanced and confined nanolight-source is created in the close vicinity of the tip apex. This nanolight-source is utilized to excite Raman scattering from a tiny volume of the sample right under the apex of the tip. (b) A SEM image of a silver-coated AFM cantilever tip. After the silver metal is coated via thermal evaporation, a thin granular silver layer is deposited on the body of the tip. The size of the tip apex is usually about 20 nm.

3. METAL FOR ENHANCED SPECTROSCOPY

Metal surfaces have abundant free electrons that move around on the surface under the influence of the forces applied by the electric fields of the neighboring electrons. At the same time, they also experience restoration forces due to their displacements under these EM forces. The free electrons usually form groups, called the plasmons, and keep oscillating collectively on the surface under the combined influence of EM and restoration forces. This collective oscillation of free electrons on a metal surface creates an oscillating EM field in the close proximity of the surface, which influences back the very electrons that created it. As a result, there is a coexistence of plasmon oscillation and an oscillating EM field near the metal surface, which is known as the surface plasmon polaritons (SPPs) or simply the polaritons.

3.1. Confined Light near a Metal Nanoparticle

Since the plasmons as well as the EM field created by them exist only near the metal surface, the SPPs are strongly confined at and bound to the surface of the metal. In fact, they are the quantum form of nonpropagating light, analogous to the photons, which are quantum form of propagating light. These SPPs propagate along the surface and their wavelength is much shorter than that of corresponding propagating photons at a given frequency. Since SPPs are also EM fields, they can interact with an external EM field, such as the propagating light, and can be resonantly excited under suitable conditions of coupling for energy transfer. However, due to the large mismatch of the momentum between the SPPs and the propagating light, the two usually do not couple efficiently for a bulk metal. On the other hand, if the metallic structure is much smaller than the wavelength of the propagating light, the conservation laws are relaxed, and the localized SPPs of a metallic nanoparticle can be resonantly excited by a propagating light, which would result in strongly enhanced evanescent light in the close proximity of the metallic nanostructure. This was first demonstrated independently by Otto[70,71] and Kretschmann[72] for thin metallic films, which are two-dimensional nanomaterials. Apart from the confinement near the metal surface, there is also a huge enhancement of this confined field due to the resonant energy transfer from the propagating light to the localized SPPs. The interaction between metal nanoparticle and propagating light therefore has a great contribution in understanding the utilization of enhanced and confined evanescent light in both SERS and TERS.

3.2. Metallic Nanotips for TERS

As discussed above, when excited with a propagating light of suitable wavelength, a metallic nanostructure can produce an enhanced and 3D confined light in the near proximity of the nanoparticle. It can therefore behave as a nanolight-source for optical measurements, such as Raman scattering in TERS. In order to perform nanoimaging in TERS, it is required to raster scan the metallic nanoparticle over the sample by means of a SPM technique, such as the STM, AFM or SFM. The spatial resolution in TERS can thus be comparable to the size of the nanolight-source, which is the same as the size of the metallic nanostructure. The metallic structures could be of any shape, such as a sphere, a nanorod, or a nanocone. The SPMs use tips (in the shapes of nanocones) as scanning probes, which are either made of a metal or can be covered with a thin layer of metal for their utilization in TERS. When the apex of a metallic or a metal-coated nanotip is illuminated with focused laser, the localized surface plasmons around the tip apex are excited, resulting in the creation of a nanolight-source at the tip apex that produces localized evanescent light. This nanolight-source works as the incident light to generate Raman scattering from a sample placed right under the tip apex. The process of Raman scattering takes place in the near-field and the spectral signal is scattered and converted back to the far-field by the tip apex, which is then collected by usual optics and spectrometer in the far-field. As the tip scans over the sample surface, the scattered signals from tiny parts of the sample right under tip apex can be collected for each point during the scan, and a spatial resolution of the order of the size of the tip apex could be obtained in the resulting image. In fact, it has been repeatedly demonstrated that much better spatial resolution than the size of the tip apex can be obtained in TERS microscopy. We will discuss the spatial resolution in TERS imaging later in this review.

4. TECHNIQUE OF TERS

Raman spectroscopy deals with both the electronic and the vibrational states of a sample and extracts rich information about the intrinsic properties of the sample. By combining the analytical strength of Raman spectroscopy and the confinement and enhancement of light near a metallic nanotip, TERS established itself as an imperative technique for nanoscale optical investigation of a variety of samples.

4.1. Optical Set-Up for TERS

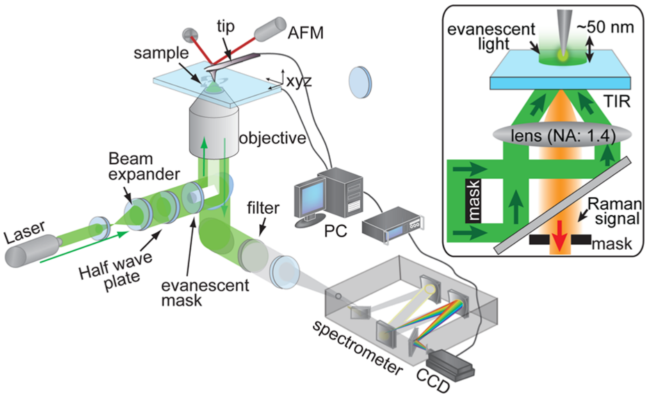

Figure 2. Illustration of a typical AFM-based TERS measurement system that consists of a laser, a high-NA inverted objective, several optical and electronic components, a spectrometer, and a CCD detector. Inset shows the details of the sample illumination process. A mask is used in the path of the expanded incident laser so that the low-NA component at the center of the beam is blocked and only high-NA component goes through the objective to create a total internal reflection at the sample substrate. This confirms that the incident light does not transmit through the substrate and the tip apex is illuminated only by the evanescent light, which drastically reduces the unwanted background signal from the propagating light. Since the evanescent light decays within a few tens of nanometers, it also assures that only the apex of the tip is illuminated to create a nanolight-source. The Raman scattered signal is collected by the same objective, and any possible reflected light is rejected by another apertured mask, that allows only the low-NA component to enter the spectrometer.

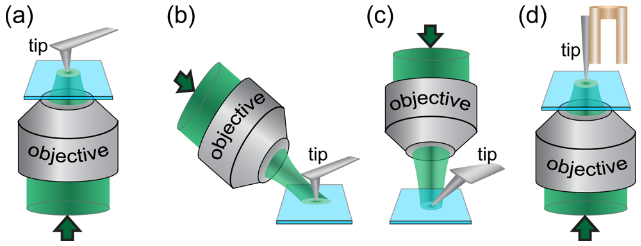

Figure 3. Some common configurations for TERS measurements. (a) Back illumination transmission mode with backscattering geometry, often used for AFM-based TERS, (b) side illumination, often used for STM-based TERS, but can also be used for AFM-based TERS, (c) top illumination, often used for AFM-based TERS with tilted tips, and (d) transmission mode for SFM-based TERS.

A schematic of the experimental setup for TERS measurement is illustrated in Figure 2, which, as in a typical Raman spectroscopy setup, consists of an excitation laser, a microscope objective usually equipped with a high-NA lens for tight focusing, a sample stage, a spectrometer, and a CCD detector. In addition, the sample stage is equipped with a SPM controller (in this case, it is a contact mode AFM) to position a metallic nanotip on the sample surface within the laser focus. Since the intensity distribution within laser focus is not uniform, it is very important to lock the relative position of laser focus and the tip.[73,74] Imaging is therefore performed by scanning the sample stage by means of Piezo controllers. There are various configurations to illuminate a sample and collect Raman signal. Figure 3 shows schematic diagrams for commonly used configurations, namely the bottom illumination that is often used in the transmission mode together with AFM controllers (Figure 3a), the side illumination (Figure 3b), and the top illumination (Figure 3c), both of which are usually utilized in the reflection mode but can be configured for transmission mode as well. In order to avoid shadow created by the cantilever, top illumination requires a titled tip, as illustrated in Figure 3c. The side illumination can be used with both AFM and STM controllers. Both side and top illuminations require objective lenses with long-working-distance. Figure 3d illustrates the bottom illumination configuration for SFM-based TERS. However, it is possible to use any of these configurations for any SPM-based TERS. Here in this review, we would mostly discuss the bottom illumination transmission mode with backscattering collection and AFM controller (Figure 3a). In this configuration, as also illustrated in the inset of Figure 2, the sample is illuminated from the bottom through an inverted microscope, the tip is placed at the top surface of the sample, and Raman scattered signal is collected in the backscattering geometry through the same microscope objective, which is then directed to the spectrometer. The sample is illuminated through an evanescent mask that blocks the central part of the laser beam and therefore cuts the low-NA component of the incident light, so that only high-NA component of the incident light at large incident angle reaches the sample. The size of the mask is adjusted in such a way that the incident angle is larger than the critical angle and hence the incident light goes through a total internal reflection (TIR) at the sample plane. This assures that no transmitted light falls on the tip and both the sample as well as the tip apex are illuminated only by the evanescent light. This reduces the unwanted background signal from the transmitted propagating light and also allows localized illumination of the tip apex, even when the length of the tip is usually of the order of tens of micrometers. The Raman scattered light is collected in the low-NA region through an apertured mask, which helps in rejecting any possible component of the reflected laser light from the high-NA regions. As the tip apex approaches the sample within the focal spot, a nanolight-source is created at the apex, which is used for the near-field measurements. TERS measurement is completed in two steps. First, Raman signal is collected by approaching the tip to the sample by means of the SPM control in the vertical direction. In this step, an enhanced Raman signal is generated from a tiny volume of the sample right below the tip excited by the nanolight-source created at the tip apex, which we refer as the near-field signal. At the same time, Raman signal is also generated from the entire focus spot due to the incident light, which we call as the far-field signal. Therefore, the signal collected in the first step is a combination of both near- and far-field Raman signals. In the second step, the tip is vertically retracted from the sample, usually by several hundred nanometers, and the Raman signal from the same area of the sample is collected. Since the tip in the second step stays far from the laser focus, there is no nanolight-source created at the tip apex. Even if the TIR of the incident light is not perfect and some leaked transmitted light generates a nanolight-source at the tip apex, it is reasonably far from the sample to excite Raman signal. Therefore, Raman signal collected in the second step contains only the far-field scattering from the focus spot of the incident light. By subtracting the signal measured in the second step from that measured in the first step, one can obtain the pure near-field Raman scattered signal. These two steps are repeated for each scanning point and a pure near-field Raman image is constructed in TERS microscopy.

As one can easily guess, the strength of TERS measurement depends on two prime characteristics of the probe tip—the abilities to enhance and to confine the light field at the apex. A major fraction of TERS research has therefore been devoted to the design and control of the tip, where researchers have tried various SPM techniques, various metals, and various deposition conditions and have tried to find the best possible design of the metallic structure on the tip apex.

4.2. SPM Techniques for TERS

As stated earlier, there are three major SPM systems used in TERS, which are based on STM, AFM, or SFM techniques. These techniques utilize different kinds of tips as the scanning probes. There are no reports on evident comparative results to clearly rank these techniques for better TERS results; however, each of them have certain advantages over the others, and the researchers have selected a particular SPM either by their expertise or by the availabilities of the systems. As discussed earlier, Figure 3 shows illustrations of typical TERS set-ups based on the three SPM technologies. The configurations in Figures 3a−c can be used for AFM, the configuration in Figure 3b can be used for STM, and that in Figure 3d can be used for the SFM controllers.

4.2.1. STM-Based TERS. In STM systems, the probe tips are made of solid metal, usually gold. It also utilizes gold substrate to control the tunneling current and the tip−sample separation. The apex of the tip is typically about 20 nm, the length is several tens of micrometers, and the tip surface is fairly smooth. Therefore, a STM tip can be best considered as a long smooth nanocone, which is not the best nanostructure to enhance visible light, because it is too long compared to the wavelength of the excitation light. However, the proximity of gold substrate in STM creates a metallic nanogap between the tip apex and the substrate, and a strongly enhanced hot spot is created within the nanogap.[34−36] Thus, a strong enhancement is achieved in STM-based TERS, which is also benefitted from the high spatial resolution associated with the STM technique. The tip plays dual roles by enhancing the light field and by controlling the tunneling current, which in turn controls the tip−sample separation, however, within the range of a few nanometers. This is not bad for usual TERS measurements, but in some applications, it might be necessary to control the tip−sample separation with larger values, which will be discussed later in this review. The recent advances of STM techniques also allow high-vacuum and low-temperature measurements,[75] which is advantageous for better stability as well as for observing samples at low temperature. Further, one can easily control the incident polarization to either parallel or perpendicular to the tip axis, if the incident light is at a grazing angle. On the negative side, since the sample is placed on a reasonably thick metallic substrate, which is opaque to the incident light, it is not possible to use the transmission mode with backscattering configuration in STM. One therefore needs to utilize the reflection mode with side illumination and side collection configuration, as illustrated in Figure 3b. Since this configuration requires a lens with long working distance, it is not possible to use objective lenses with high-NA, and hence it is not possible to tightly focus the incident light on the tip apex. Some groups have used an interesting optical system for STM, where, instead of a lens, they use a parabolic mirror to focus the incident light to the tip apex as well as to collect the Raman signal.[75,76] This configuration allows them to slightly improve the size of the focus spot.

4.2.2. AFM-Based TERS. The scanning probes used in AFM are semiconductor cantilever tips and the apex of these tips are usually very sharp with an apex diameter of about 5 nm or less. These tips are covered with metal, commonly by thermal evaporation under high vacuum[77] or electroless plating[78] techniques. It is possible to choose the coating material from a variety of metals ranging from tungsten, gold, silver, to aluminum, which enables one to control the range of plasmon resonance. One can control the thickness of the coated metal and the size of the tip apex, which is usually kept at about 20 nm. AFM tips can be used in either bottom illumination (Figure 3a) or in side/top, illumination (Figure 3b,c) configurations, however, the former being more common. One major difference between AFM tips and STM tips is that the surface of the tip for AFM-based TERS is rough because the coating process deposits nanoparticle-like structures on the surface of the semiconducting tip. These nanostructures are much smaller than the wavelength and are thus suitable for the resonant excitation of SPPs. The tip alone creates a strong hot spot near the apex and a metal substrate is not required for the same. However, a thin metal substrate can be optionally used to further enhance the field in the nanogap, which can be thin enough to be transparent.[79] The nanostructure attached right at the tip apex during metal deposition process plays the most important role in field enhancement. Unlike in the STM tips, here it is possible to control the resonance wavelength by adjusting the size of the nanoparticles, which can be advantageous when one needs to tune the resonance in certain experiments. Researchers have devoted a reasonable amount of effort in optimizing the deposition process to obtain the best results in resonant enhancement and strong confinement of light. Since a metallic substrate is not necessary, the sample can be placed on a glass substrate and the tip apex can be illuminated in the transmission mode geometry, as shown in Figure 3a. The major advantage of this configuration is that one can use short-working-distance high-NA objective lenses to tightly focus the incident light and to collect the Raman scattered light. High-NA objectives also allow one to use the evanescent illumination to ensure that only the metal nanostructure attached at the apex of the tip is selectively illuminated, as in the inset of Figure 2.

The field distribution within the focus spot depends on the polarization of the incident light.[73] When the incident light has radial polarization, the light intensity at the focus spot has a Gaussian distribution with maximum intensity at the center. On the other hand, when the incident light has linear polarization, the intensity distribution at the focus spot has a doughnut shape with two maxima along the diameter. In order to get best results, it is extremely important to position the tip apex at the point where the intensity is maximum, and lock the relative position of the focus and the tip apex. Owing to the large incidence angle for high-NA objective lenses, one can create a polarization parallel to the tip apex, in addition to the in-plane linear and radial polarizations, which is suitable for polarization-dependent TERS measurements. This is usually done by utilizing a certain arrangement of polarizers, such as in z-pol.[80]

AFM has two modes of operation, namely the contact mode and the tapping mode. Since the tip mostly remains away from the sample in tapping mode, the contact mode is most commonly used for TERS measurements. In contact mode operation, the tip is always in contact with the sample making the tip−sample separation zero. This is good for better enhancement. However, in some experiments, it is interesting to precisely control the tip−sample separation over a wide range. By utilizing the tapping mode operation and time-gating technique, it is possible to precisely control the tip−sample separation from a few angstroms to more than 100 nm.[81,82] This method of controlling tip−sample separation will be discussed later in this review. Although there are several reports on tip−sample separation dependent TERS with STM- and SFM-based systems,[83−87] such a high precision has only been demonstrated for AFM-based TERS.

With recent developments in the AFM technique, it has become possible to operate AFM in liquid environment, where the entire tip, the cantilever, and the sample are immersed in a liquid. This is an interesting development, particularly for biological samples, because it allows the nanoinvestigation of native biomaterials in aqueous environment under physiologically pertinent conditions. Following this, some researchers have reported TERS measurements in liquid environment, particularly in water,[88−90] which is suitable for biological samples to remain alive and continue their physiological activities during the measurement. On the other hand, TERS in liquid for STM-based system would require a suitable coating on the tip so that the Faradaic current does not interferes with the tunneling current and also a suitable liquid is required to maintain the tunneling current. Although a few reports on electrochemical TERS (EC-TERS) in STM-based system have been reported,[91−94] where STM tip was immerged in liquid chemicals suitable for the function of STM, the liquid used may not be suitable for maintaining physiological activities of biological samples. Perhaps for this reason, no TERS image of biological sample in STM-based liquid TERS has been reported so far. Thus, AFM-based TERS appear to have an edge over STM-based TERS for the measurements of live biosamples. However, currently it is not possible to have a high-vacuum and low-temperature environment for AFM-based TERS, where the STM-based TERS gets an upper edge.

4.2.3. SFM-Based TERS. The third scanning technique, namely SFM, is also one kind of AFM, where the tip is attached to one of the prongs of a quartz tuning fork that vibrates parallel to the sample substrate (Figure 3d). Although a very few research groups use SFM-based TERS, they have shown remarkable results.[95−97] SFM-based TERS also utilizes a probe tip made of a solid metal, which are usually fabricated by chemical etching of metallic nanowires. Often gold or silver nanowire have been used to fabricate SFM tips and the typical size of the tip apex is of the same order as in the other TERS techniques. Both bottom and side illumination configurations can be used and the tip−sample separation is maintained through the shear-force feedback controller, which is typically of the order of a few nanometers. Apart from these, all other properties of SFM-based TERS system are similar to those for the AFM-based TERS system.

In addition, some groups have also tried to attach a metallic nanoparticle to the apex of the scanning probes or to fabricate a small nanostructure right at the tip apex.[98−100] This is suitable for the experiments where one needs a narrow and sharp plasmon resonance. Later in this review, we will discuss some tips with small metal structure fabricated at the tip apex.

4.3. Controlling Plasmon Resonance of the Tip

As discussed above, there are various kinds of tips used in different TERS configurations. Here, we will focus on the AFM-based TERS systems and will discuss about a variety of tips that researchers have utilized in AFM-based TERS measurements. The choice has been mostly driven from the need of precisely controlling the plasmon resonance and improving the enhancement factor.

4.3.1. Choice of the Metal. The tips for AFM-based TERS are typically fabricated by thermal evaporation of gold, silver, or aluminum on a commercially available silicon AFM cantilever tip. The choice of metal depends on the requirement of the plasmon resonance wavelength. While gold shows strong enhancement for longer wavelengths in the red spectral region, silver shows better results in the blue-green spectral region, and aluminum shows promising results for the enhancement in the UV and deep UV spectral regions. Since gold is very stable under the ambient condition, gold-coated tips can survive for a long time. On the other hand, silver can easily get oxidized and hence the silver-coated tips can lose the plasmonic enhancement within a few hours. There have been several attempts to protect the silver-coated tips from oxidation by storing them in either inert environment or in a suitable chemical environment. However, they still get oxidized during the measurement process and hence can be used only for a few hours. There have also been some attempts to cover silver-coated tips by coating a thin layer of a transparent material, such as silicon dioxide or aluminum oxide, so that they can last long during the measurement process.[101] Aluminum also gets oxidized quickly, however, oxidization stops after a thin layer (about 2 nm) of aluminum oxide is formed on the tip surface, and hence aluminum-coated tips are naturally protected and survive much longer than the silver-coated tips.[102] Nevertheless, due to strong enhancement in the blue-green spectral region, which is the favorite spectral region of Raman spectroscopists, silver-coated tips are the most commonly used tips in AFM-based TERS experiments. STM-based TERS often uses a solid gold tip.

4.3.2. Choice of the Base Material. AFM cantilever tips are usually made of semiconductors, mostly silicon. One can also play around with the base material of the cantilever to control the refractive index and hence the plasmon resonance. This can be done by, for example, preoxidation of the silicon cantilever by heating the cantilever tip to a high temperature (∼1000 °C) in the presence of water vapor. This process converts the base material of cantilever into silicon dioxide with lower refractive index than silicon, resulting in a blue shift of the plasmon resonance.[103] One can very precisely control the plasmon resonance in a wide spectral region by regulating the oxidation time, which determines the thickness of the oxidized layer. In the early days of TERS, Fischer's group employed a

DOI: 10.1021/acs.chemrev.6b00821
Chem. Rev. 2017, 117, 6447−6466

piece of sharp edged glass as the base material,[104,105] and Levis et al. used tips made of glass.[106] These tips also have lower refractive indices than silicon and show better plasmon resonance in the shorter wavelength region.

4.3.3. Structure of Evaporated Metal.

The plasmon resonance wavelength as well as the enhancement factor of a tip strongly depends on the structure or the morphology of evaporated metal on the tip surface. It has been realized both in simulation and in experiment that a tip coated with smooth metal film does not show strong enhancement in the visible region. This is because the resonance wavelength of SPP oscillations in a long and smooth tip would also be long, which would have a weak plasmon-photon coupling in the visible region. It should be noted that even without a strong plasmon resonance, a smooth and sharp tip can still have reasonable amount of enhancement due to the lightning rod effect, which is basically independent of the incident frequency.

Several authors have been using tips with roughened or corrugated metal coated surfaces for better results, but not many investigated the extent up to which the rough surfaces with metallic nanostructures are better than smooth surfaces.[74,107] A recent report discusses this issue in a great detail, where the authors investigated the effect of multiple metal grains on the enhancement of TERS signal.[108] The authors compared the enhancement for a tip that had smooth surface with that for a tip that had nanostructured surface, both in experiment and in simulation. A noticeable difference in enhancement factor was observed, which confirmed that granular morphology of the surface of a tip is necessary for obtaining good resonance in the visible range. The metal nanostructures or the grains on the surface of a tip work as resonant dipole antennas, which efficiently couple the optical radiation between far-field and near-field. The resonance wavelength of these optical antennas is predominantly determined by the size of the grains, where the grain size is comparable to the wavelength of SPPs. Note that the wavelength of the SPPs is much shorter than that of the propagating light for a given frequency.[109]

The authors considered a silver-coated tip that was corrugated with hemispherical silver grains with a diameter of 40 nm. In the simulation, they considered only a certain number of such silver grains attached at and around the tip apex. The result showed that the enhancement strongly depended on the number of grains and there was an optimal number of grains for best enhancement. The other important observation was that when the grains are disconnected with a grain to grain separation of about 4 nm, the enhancement was significantly larger compared to the case were the grains were connected to their neighboring grains. In addition to larger enhancement, a noticeable spectral broadening was observed for disconnected grains, which is beneficial for simultaneous enhancement of both incident and Raman scattered light. These results were also confirmed experimentally.

Although multiple metal grains near the tip apex provide good enhancement, it is observed that even a single nanoparticle attached to the tip apex works well. Several authors have shown interest in fabricating a tip with a single metallic nanoparticle attached to the tip apex.[97,110] Since tips with long and smooth metal surface behave like a long antenna and are not suitable for resonant enhancement in the visible region, researchers got motivated to try smaller antennas, of the order of 100−200 nm in length. Attaching a metal nanoparticle to the tip apex was one such attempt. In a different approach, the authors used photochemical technique to grow a silver nanospheres right at the tip apex (Figure 4a) and showed a 20 times better enhancement compared to the regular TERS tips.[111] They could easily control the size of the nanoparticle by adjusting the growth parameters. Figure 4b shows a SEM image of a silver particle grown on the tip apex with size under 100 nm. In another report, the authors utilized the techniques of focus ion beam to first mill the base material to control the size of the region where metal could be deposited, and then they evaporated silver on the milled structure.[112] This created a small silver nanostructure at the tip apex, as shown by the SEM image in Figure 4c. The authors demonstrated a fine control over the plasmon resonance wavelength by controlling the length of the nanostructure.

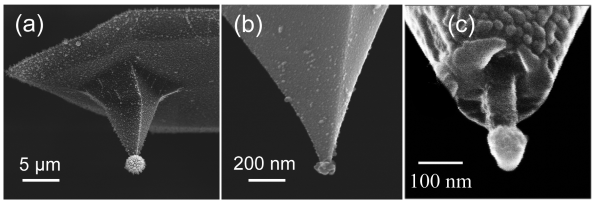

Figure 4. Nanosized metal particle at the tip apex. (a) A silver microsphere is directly grown at the end of the tip apex using photochemical technique. (b) The size of the photochemically grown spheres can be controlled down to sub-100 nm size. (c) A silicon tip was first milled to a mushroom shape by FIB milling, and then silver was thermally evaporated. As a result, and small metallic particle was deposited at the tip apex. The size of metal particle can be easily controlled. Reproduced with permission (a) and (b) from ref 111. Copyright 2012 The Japan Society of Applied Physics and (c) from ref 112. Copyright 2015 The Japan Society of Applied Physics.

In another interesting attempt to improve the signal-to-noise ratio in TERS, some authors proposed to utilize the phenomenon of plasmon nanofocusing.[113−115] In this technique, the laser is focused on the upper area of the tip, far from the apex, and hence far from the sample, usually at a distance of about 10 μm. A light-plasmon coupler in the form of a grating is fabricated at this spot, where the focused propagating light can get coupled with the local plasmons of the tip. The excited plasmons then travel toward the tip apex through the process of adiabatic compression and create a huge confined field at the tip apex.[113] This process is known as the plasmon nanofocusing. Since the incident laser and the nanolight created by adiabatic compression are spatially separated, there is no far-field background. Near-field imaging can therefore be done with high signal-to-noise ratio.[115]

Nevertheless, the most commonly used tips for AFM-based TERS are the tips that have disconnected metal nanoparticles evaporated on a semiconductor cantilever. Every group optimizes the evaporation parameters in their own way to obtain best possible results, both in enhancement and in controlling the plasmon resonance wavelength. Figure 5a shows the SEM image of such a tip that has disconnected silver nanostructures deposited on its surface. The inset shows an illustration of the concept.[108]

5. APPLICATIONS OF TERS

Since TERS extends the sensitivity as well as the spatial resolution to a completely different level in comparison to the conventional Raman measurements, it immediately found its utilization in the investigation of a variety of nanostructured

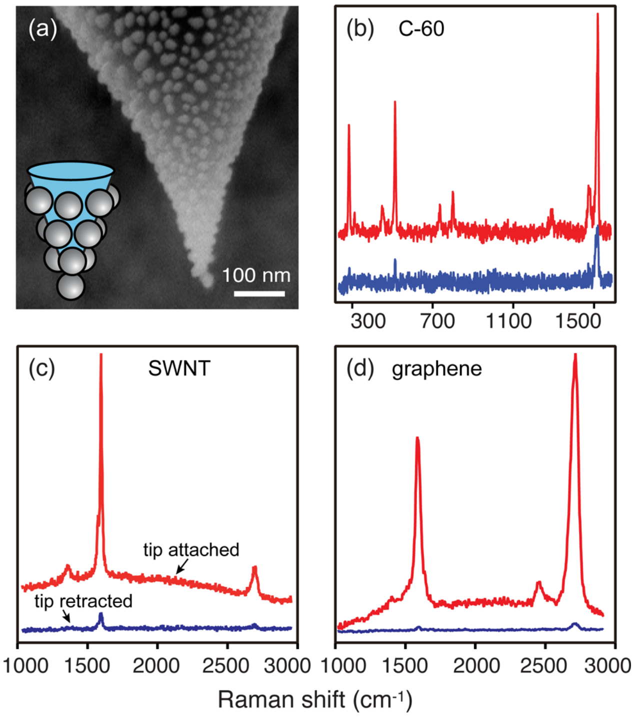

Figure 5. (a) SEM image of the silver-evaporated nanotip, where the deposited silver particles are disconnected, as illustrated in the inset. TERS spectra measured from (b) carbon-60, (c) single-walled carbon nanotubes, and (d) graphene. Upper red curves in b−d represent the near field spectra when tip was in contact with the sample, while the blue curves represent the far-field spectra when the tip was retracted. Panels a, c, and d are reproduced from ref 108 by permission of The Royal Society of Chemistry. Panel b is reproduced with permission from ref 116. Copyright 2006 APS.

materials, ranging from organic and chemical substances to the biological samples. TERS has provided an insight into the structure and chemistry of these sample at nanometer scale that is not possible to obtain by any conventional optical or analytical methods. We will discuss a few examples to underline the applications of TERS.

5.1. TERS for Carbon Materials

Among many other nanomaterials, carbon materials, such as carbon 60 (C60), single-walled carbon nanotubes (SWNTs), and graphene provide interesting samples for TERS measurements. Figure 5b−d show examples of TERS measurement from a nanocluster of C60,[117] thin bundles of SWNTs, and a graphene sample,[108] respectively, which were measured with tips similar to the one shown in Figure 5a. The lower spectra for all samples correspond to the far-field measurement where the tip was retracted from the sample, while the upper spectra correspond to the near-field measurements where the tip was in contact with the sample. When the tip is retracted from the sample, there is no confined light near the sample and thus no enhancement is observed in the lower spectra. These spectra represent usual far-field Raman scattering, which is quite weak due to the small volume of the samples. When the tip comes in contact with the sample, the tip apex enhances both incident and Raman scattered light from the sample right under the tip (upper spectra). The far-field Raman scattering in the lower spectra are generated from the sample volume within the diffraction-limited focal spot. On the other hand, the enhanced scattering in upper spectra represents the combination of this far-field Raman scattering together with the near-field Raman scattering generated from a nanometric volume of the sample that is immersed into the confined field at the tip apex. Subtraction of the lower spectra from the upper spectra would provide the intensity of the pure near-field Raman scattering. Enhancement factor in TERS is defined as the ratio between pure near-field and far-field Raman intensities per unit volume. Taking the near-field and the far-field excitation volumes into consideration, one can calculate the enhancement factor from the intensity ratio. The enhancement factors in Figure 5 are of the order of 10^3−10^5. A simple comparison just by looking at the lower and upper spectra in Figure 5b−d highlights the importance of TERS technique for the optical investigation of nanosized samples.

5.1.1. Nanoimaging of SWNTs with TERS. Due to their ideal one-dimensional structure, SWNTs are attractive samples for the demonstration of the potentials of TERS measurements. SWNTs have remarkable chiral, mechanical, thermal, and electronic properties with nanometric structure, which has attracted great interest in TERS community. Since one of the most significant features of TERS is the high spatial resolution, SWNTs with one-dimensional structure are the best samples to explore the extent of this feature. Figure 6a shows a high resolution TERS image of a thin bundle of SWNTs, and Figure 6b shows simultaneously obtained AFM image for comparison.[108]

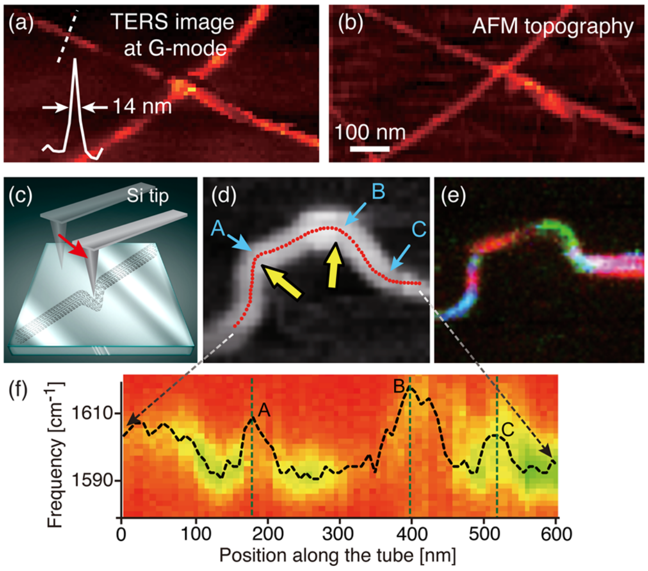

Figure 6. (a) Example of TERS image of a sample that contained two thin bundles of SWNTs. This image was constructed from the intensity of the G-mode. Inset shows the intensity line-profile along the white dotted line, confirming the spatial resolution of about 14 nm. (b) A corresponding AFM image measured simultaneously with the TERS image. (c) An illustration of lateral dragging of a SWNT with a silicon tip. (d) AFM image of a manipulated SWNT after it was dragged along the yellow arrows. The points marked by the letters A, B, and C had smallest curvatures after the nanotube was manipulated. (e) Color-coded TERS image of the same sample, constructed from the shift in G-mode frequency, where color indicates shifts and represents the variation of strain along the length of the nanotube. (f) Shift in the G-mode frequency along the red dotted line in (d). Panels a and b are reproduced from ref 108 by permission of The Royal Society of Chemistry. Panels c−f are reproduced with permission from ref 117. Copyright 2013 NPG.

High spatial resolution in optical imaging is of tremendous importance, because it does not only image the topography of the sample, but also its intrinsic properties. For example, one can scan the tip along the length of an isolated SWNT and investigate any intrinsic property of the SWNT along its length. Yano et al. demonstrated the measurement of localized strain along the length of an isolated SWNT.[117] The authors casted an isolated SWNT on a glass substrate, and dragged the nanotube laterally by means of a silicon AFM tip, as illustrated in Figure 6c. They could fold the nanotube into many different shapes by applying lateral force at different locations. One such example is shown by AFM image of a manipulated SWNT in Figure 6d, where the nanotube was dragged along the yellow arrows. The dragging process has two effects on the nanotube, rolling and elongation, which create localized torsional and tensile stress, respectively. Which out of the two dominates, depends on the location of the tip that drags the nanotube and on the strength of adhesion of the nanotube on the substrate. Interestingly, the torsional and the tensile strains result in a shift of the G^+-mode of SWNT in opposite directions. Therefore, by looking at the shift of the G^+-mode in TERS measurement along the length of a manipulated SWNT, one can estimate the variation in the strain along the length. This is shown by the color-coded TERS image in Figure 6e, where the color represents shift in the G^+-mode. The authors measure TERS along the red dotted line in Figure 6d and observed the variation in the G^+-mode frequency, which is plotted in Figure 6f. The regions with small curvatures, marked by the points A, B, and C, show larger shifts than the regions with large curvatures. The authors also manipulated an isolated SWNT in the shape of the letters "CNT", and discussed the strain developed along the nanotube due to elongation and rolling. In a similar fashion, one can also image various other properties, such as the chirality or the defects, along the length of an isolated SWNT at high spatial resolution. Obviously, this study can be extended to other samples to construct nanoimages of any physical or chemical properties in one or two dimensions. This interesting work demonstrates the strength of TERS that can optically image an intrinsic property of a sample at nanoscale.

In another example of imaging the physical property of a carbon canotube sample at nanoscale, the authors demonstrated mapping of diameter distribution of nanotubes in a sample that contained bundled SWNTs.[118] Figure 7a shows a confocal far-field Raman spectrum of a sample that contains various kinds of SWNTs in a bundled form. The spectral range corresponds to the radial breathing mode (RBM) of SWNTs. Since the position of RBM is inversely proportional to the diameter of the nanotube, the appearance of several peaks in this spectral region confirms that the bundle contains nanotubes with different diameters, as schematically shown in Figure 7b. The authors selected three distinct RBM peaks, marked by three colored bars in Figure 7a, which correspond to nanotubes with the diameter of 1.23, 0.97, and 0.85 nm, respectively. TERS images constructed from the intensity of these three peaks are shown in Figure 7c−e, which reveals how the diameter of nanotubes, indicated in each figure, is distributed within the bundle. It can be even better visualized in the overlapped image shown in Figure 7f, where the color-coded diameter distribution can be observed with nanoscale resolution. Similar nanoimaging for a spatial distribution of any other physical or chemical properties of a sample could be realized by TERS. Clearly, this kind of information at nanoscale resolution is not possible by conventional Raman spectroscopy.

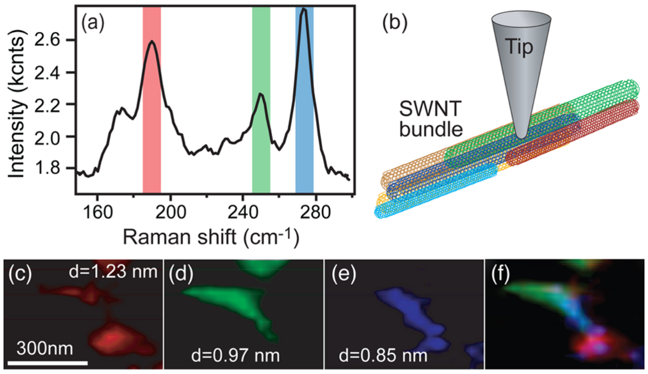

Figure 7. (a) Far-field Raman spectrum of a bundle of SWNT in the RBM spectral region. Each peak in the spectrum corresponds to a specific diameter of the nanotube present in the bundle. (b) A schematic representation of different kind of nanotubes constituting a bundle. (c−e) TERS image of the SWNT bundle constructed from the intensities of three different RBMs indicated by three color bars in panel a, respectively. The corresponding diameters are indicated in the figures. These TERS images represent the distribution of the corresponding diameters in the sample. (f) TERS image constructed by merging the images in panel c−e. This color-coded TERS image shows the variation of the diameter of nanotubes within the bundle at nanoscale, where the color variation represents the variation in diameters. Reproduced with permission from ref 118. Copyright 2006 IOP.

5.2. TERS for Biological Materials

While carbon nanotubes and other carbon materials are probably the most investigated samples by TERS, lately various biological materials and biomolecules have also received great attention. Several biological samples, such as specific molecules,[119] viruses,[120] bacteria,[121] erythrocytes,[122] and cellular systems[123] have been studied and nanoanalyzed by TERS.

There are some interesting studies on the nucleic acids, such as the DNA and RNA.[124] The earlier TERS investigations of DNA base nanocrystals[125−128] demonstrated that it was possible to distinguish the respective nucleobases, which then led to the successful TERS investigation of a single RNA strand of a cytosine homopolymer.[124] Deckert's group recently demonstrated TERS measurement of an insulin fibril, where the authors revealed direct molecular distinction of selected amino acids.[129] They measured TERS spectra along an insulin fibril with a step size of 0.5 nm between two consecutive tip locations and demonstrated that the spectra were distinct with characteristics of different amino acids. From this result, the authors also claimed a spatial resolution of 1−2 nm in their TERS measurement, although, they did not construct any image.

Another interesting biological sample for TERS investigation are the pathogens, such as bacteria and viruses. TERS can deliver nanoscale chemical information from the surface of pathogens, which can provide localized composition of specific components. Several biological processes, such as the bacterial adhesion, bacterial pathogenesis, or the formation of biofilms can be well investigated through TERS at the nanoscale.[120,121] Neugebauer et al.[121] reported TERS measurements from a bacterial surface for the first time, where they could enhance the fingerprint Raman modes of peptides and polysaccharides. By identifying the temporal variation in TERS intensity at the same location, the authors claimed detecting the protein dynamics at the cell surface. This demonstrates the possibility of studying complex biological systems at the nanoscale using TERS.

Furthermore, it was demonstrated that TERS can be applied to probe hemozoin crystals. Wood et al. showed the characteristic hemozoin bands by measuring the digestive vacuole of a sectioned malaria parasite infected red blood cell.[122] TERS also shows promising results from lipids,[90] which are the fundamental building blocks of biological cell membranes. Lipids also facilitate the interaction of a cell with its external environment such as pathogens or drugs. TERS provides label-free chemical imaging of phase-separated lipid domains and could be used for the nanoscale investigation of cell membranes.[130−132]

The application of TERS in studying biological samples has recently been rapidly increasing. However, in order to fully exploit the potentials of TERS, further refinement of the technique is necessary. For example, TERS measurements in liquid is a boon for studying biological samples under their native physiological conditions, which is still in its premature stage. Also, since these samples are usually soft, TERS based on noncontact mode of AFM would avoid tip-related damages to these samples. Tips with much higher enhancements would better suit the biological samples that need to be measured with low laser intensities.

5.3. TERS for Various Other Materials

Apart from carbon materials and biological samples, full advantages of TERS has also been taken to study catalysts, polymers, organic solar cells, semiconductors, and other materials.[133−139] Many chemical and biological activates are often confined to nanometric sites, and hence, they can be best revealed with TERS.

For example, the whole process of photophysics in an organic solar cell depends on the nanoscale morphology of the active material that determines the efficiency of the charge transport. Researchers have successfully utilized TERS for the chemical mapping of the organic components and their morphologies in solar cells.[140] Several polymers and polymer blends have also been successfully studied with TERS at nanoscale.

Similarly, catalysts have versatile usage in our lives and thus have been important subject of study for the chemists. It is well-known that the catalytically active surfaces are heterogeneous at nanoscale, and hence the identification and measurement of their local properties at high spatial resolution is of great interest. TERS naturally stands out as one of the best tools to investigate the chemical reactions and to monitor the molecular dynamics occurring at catalytically active sites. In an interesting report,[141] authors utilized a silver-coated nanotip as both, a catalytic site where the photocatalytic reduction took place at the apex, as well as a TERS tip to enhance Raman scattering at the same time.

These are just a few examples of the application of TERS in understanding and visualizing some interesting science at the nanoscale. TERS has recently seen its application in several interesting fields.[142−151]

5.4. Super Spatial Resolution in TERS

As discussed so far, one can achieve extremely high spatial resolution in TERS, far beyond the diffraction limit of the probing light. Naturally, the researchers were interested in finding the best possible resolution and a fair amount of research was dedicated to push this limit. It was predicted from the theory that the size of the confined light near the tip apex is typically of the same size as the tip apex, thus the best achievable spatial resolution was expected to be the same as the size of the tip apex. In the early days of TERS, Novotny's group demonstrated a spatial resolution of 25 nm for a SWNT sample, which was comparable to the size of the tip apex.[96] However, later as the TERS technique matured, the value of spatial resolution achievable by this technique also improved.[152−155] Figure 6a shows an example of high spatial resolution TERS image from a recent publication where the authors used a sample that contains two thin SWNTs bundles.[108] This image was constructed from the intensity of the G-band vibrational mode of SWNT, where a high spatial resolution of 14 nm was observed, as seen from the intensity line profile along the dotted line in the inset, while the tip apex was larger than 20 nm. For a comparison, Figure 6b shows a corresponding AFM image obtained simultaneously with the TERS measurement. In fact, there were several other reports demonstrating a spatial resolution much smaller than the size of the tip apex. Though, in many cases the origin of this super resolution remained debated. Yu et al.[82] showed a spatial resolution of 8 nm, however, with a special technique of tapping mode AFM, where they could in situ remove the far-field background and measure pure near-field. Recent publications have often shown a spatial resolution around 10 nm, thus one can safely say that it is possible to achieve a high spatial resolution of about 10 nm in modern TERS. Although, there have been a few reports claiming extremely high resolution of molecular or even submolecular size. For example, Deckert's group investigated amyloid fibrils with TERS using a step size of 0.5 nm, and found pronounced spectral changes, which they assigned to the spatial variation in sample composition.[156] The authors claimed a spatial resolution of about 1 nm.[156−158] In a recent report, Zhang et al. demonstrated chemical mapping of a single molecule using STM-based TERS and claimed a subnanometer spatial resolution.[159] The same group also claimed subnanometer resolution for carbon nanotubes in another publication.[160] These recent experimental demonstrations clearly show that a spatial resolution of molecular and submolecular level can be achieved; however, the origin of this super high resolution is still under debate. In a very recent publication, Deckert's group discussed that a molecular size protrusion on the tip apex maybe responsible for such a high resolution.[161] A technique combining TERS and tip-applied localized pressure was demonstrated a few years ago, where a spatial resolution of 3−4 nm was claimed for CNT[81,162] as well as for DNA[162] samples. Here, the mechanism of achieving super high resolution was well explained through the effect of tip-applied localized pressure, which will be discussed in more details later in this review. Even though there have been discussions on some of these claims, it is not surprising if TERS established itself as a technique for true nanoscale optical measurement with high reproducibility in the near future.

6. ADVANCED TECHNOLOGIES IN TERS

With extensive experiences, growing expertise, improved instrumentations, and enriched understanding about TERS mechanism, we have witnessed remarkable advances in the application of TERS that addresses specific issues and provides better understanding and control over the expected results at nanoscale. For example, controlling polarization of the confined light at the tip apex would allow nanoscale investigation of the polarization dependence for those samples that are sensitive to the polarization. Similarly, controlling precisely the tip−sample distance or the tip-applied localized pressure on the sample surface would allow one to focus on some specific issues that can be addressed only in TERS. Here in this section, we will discuss some interesting additions to the established technique of TERS that brings TERS to a new level as an indispensable technique for nanoinvestigation of various materials.

6.1. Polarization in TERS

Polarization-dependent TERS investigation allows one to study highly directional intrinsic properties of a sample at the nanoscale. However, unlike in the far-field illumination where one can use a set of polarizers to control and measure polarization, neither evaluation nor control of the polarization properties of the near-field light in TERS is as straightforward. This is because the metallic nanostructure attached to the tip apex, which is responsible for generating the near-field light and hence its polarization, is usually random in shape, size, and orientation. One can still control the near-field polarization, up to certain extent, by precise control on the polarization of the incident light.[74,163] SWNT is one of the best samples to study polarization effects because, it not only has a one-dimensional structure, but also because its two prominent Raman modes, namely the RBM and the G-mode are in the radial and axial directions, respectively. It was demonstrated a few years ago that one can selectively enhance either RBM or G-mode by switching the incident polarization parallel to the mode oscillation.[80,164] Figure 8a,b shows selective enhancements of RBM and G-mode vibrations of a SWNT sample under dominant *p*- and dominant *s*-polarizations, respectively, where *p*-polarization means incident polarization parallel to the tip axis and *s*-polarization means incident polarization in-place with the sample. Although the near-field polarization is not purely governed by the incident polarization, it can still be controlled up to certain extent by controlling the incident polarization. Since RBM vibrations are in the radial directions, they can be selectively enhanced by the *p*-polarization, and on the other hand, the G-mode vibrations are parallel to the nanotubes, hence they can be selectively enhanced by the *s*-polarization. This is a nice demonstration of selective enhancement of a particular vibrational mode in TERS by controlling the incident polarization. This method is useful for high-resolution TERS imaging, particularly when two or more vibrational modes with different responses to polarization lie in close proximity, where it is possible to selectively enhance only one mode out of several modes.

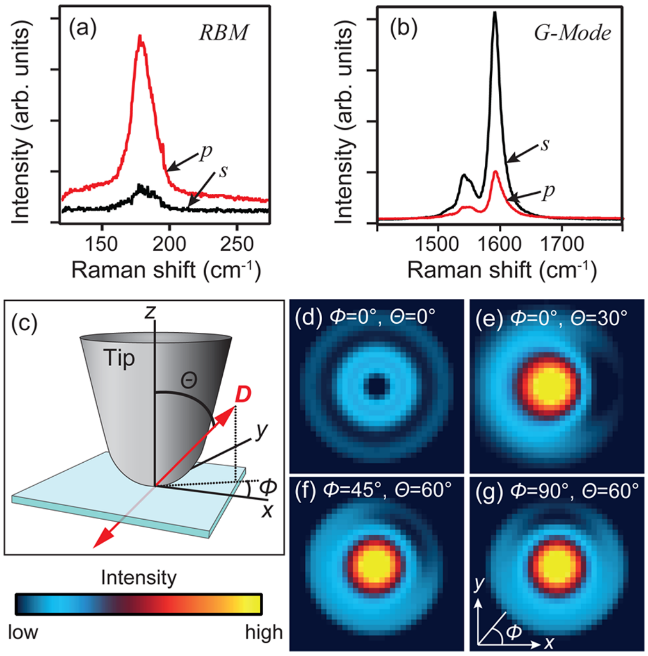

Figure 8. (a,b) Polarization dependent TERS spectra of SWNT in RBM and G-mode spectral regions, respectively. While the RBM is selectively enhanced under *p*-polarization (red line), the G-mode is selectively enhanced under *s*-polarization (black line). (c) Near-field polarization depends on the dipole moment generated at the tip apex. The schematic shows the spatial coordinate system at the tip apex and the definition of tilt and twist angles (Θ, Φ) for the dipole orientation. (d−g) Calculated defocused image patterns for several dipole orientations. The location and the size of the black crescent defines the near-field polarization around the tip apex. (a) and (b) are reproduced with permission from ref 164. Copyright 2010 John Wiley & Sons, Inc. Panels c−g are reproduced with permission from ref 165. Copyright 2014 American Chemical Society.

In a more detailed study, the authors considered the role of a metallic nanostructure attached right at the tip apex and demonstrated the effect of near-field polarization in TERS.[165] In this study, the polarization of the incident light was fixed, and the role of the nanostructure at the tip apex was studied. They assumed that the illumination of this metallic nanostructure generates a single dipole, where the oscillation direction of the generated dipole determines the polarization of the near-field light near the tip apex. The best way to evaluate a tip is to measure its scattering pattern. The direction of dipole oscillation can be determined from the asymmetry in the scattering pattern, because the light emitted from a dipole in the direction perpendicular to the dipole is stronger than that in the parallel direction, resulting in an asymmetry in the scattering pattern.[166,167] Figure 8c shows the schematic of the dipole generated at the tip apex. The $x-y$ plane is defined as the sample plane and the z-axis as the direction of propagation of the incident light, which is perpendicular to the sample plane. Vector $\boldsymbol{D}$ shows the direction of the dipole oscillation and is described by the tilt angle Θ, which is the angle between the dipole axis and the z-axis, and the twist angle Φ, which is the angle between the x-axis and the in-plane component of the dipole $(\boldsymbol{D}_x + \boldsymbol{D}_y)$. The authors investigated the direction of oscillation of the dipole generated at the tip apex by using so-called defocused imaging technique.[168] This is because the directional information is lost when the scattered light is well focused. On the other hand, this information remains intact at a plane away from the focal plane. For $\Theta = 0$, which means the dipole is in the z-direction, the defocused pattern has a doughnut shape with a dark center, as can be seen in Figure 8d. For increased values of Θ and Φ, the dark area in the center moves to the side and takes the shape of a crescent (Figure 8e−g). The size and locations of this dark crescent determines the direction of near-field polarization.

The authors fabricated three different tips and evaluated the direction of near-field polarization for each from the corresponding defocused images of the scattering patterns. After evaluating the polarization, they measured TERS images from SWNTs and confirmed that the image contrast depended on the direction of the dipole oscillation, verifying that the polarization of the near-field was quantitatively estimated by their technique. Later, the authors combined both the

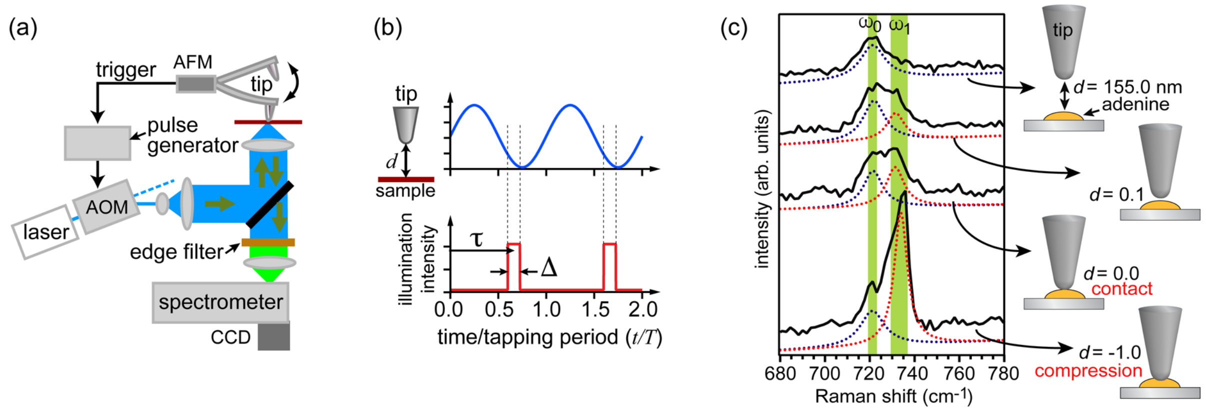

Figure 9. (a) Schematic of modified TERS system using a tapping-mode AFM and acousto-optic modulator for time-gated illumination. (b) Illustration of a sinusoidal oscillation of the tip and the synchronized opening of the time gate. The tip−sample separation d and the resolution in the distance can be selected by choosing certain values of τ and Δ. (c) Raman spectra of an adenine nanocrystal at various tip−sample separations, indicated in the corresponding insets. The peaks marked by ω_0 and ω_1 represent the unperturbed and the frequency-shifted components RBM, respectively. Reproduced with permission from ref 81. Copyright 2009 APS.

estimated near-field polarization from the scattering pattern of a tip and the polarization control by controlling the incident polarization, to realize the best possible understanding of the polarization in TERS.[163]

A more detailed discussion on polarization in TERS can be found in a recent mini-review by Schuck et al.,[169] where the authors discuss the recent progress and provide a perspective on the emerging directions for utilizing and controlling in-plane optical polarization and highlight some key applications.

6.2. Tip−Sample Separation Control

In the recent past, we witnessed a noticeable technological development[81] in TERS, where the authors achieved subnanometer control on the tip−sample separation. Since the tip−sample interaction in TERS strongly depends on their separation, a precise control on the tip−sample separation can address important chemical and physical issues involved in TERS process.

Researchers have often payed attention only to the electromagnetic interaction between the tip and the sample. However, when the tip−sample separation is small, particularly of the order of molecular distances, the chemical and mechanical interactions between the metal atoms on the tip and the sample atoms becomes important. When silver atoms of the tip come in contact with the sample molecules, a chemical bonding or charge transfer can significantly modify the Raman scattering. Similarly, if any silver molecule on the tip apex presses against the sample molecule, Raman modes can be modified from the perturbed sample molecules. Therefore, in the contact-mode AFM-based TERS measurements, the enhanced Raman signal can be a complex mixture of electromagnetic, chemical, and mechanical interactions, which can potentially make it difficult to precisely interpret TERS data. Therefore, understanding and separating different effects of tip−sample separation on TERS is of scientific as well as practical importance. Fortunately, the interaction ranges of these three interactions are very different from one another; therefore, it is possible to distinctly measure them, if the tip−sample separation can be precisely controlled.

Among a few others,[170,171] the tapping mode AFM has advantage in precision and stability in controlling the tip−sample separation.[81,172] In this scheme, the tip−sample separation-dependent TERS can be measured through a narrow time gate that is accurately synchronized with the tapping oscillation. By sweeping the time gate across the entire oscillation period, one can cover the entire region of tip−sample separation within the tapping amplitude. This can be done either by time-gating the detection signal[172] or by time-gating the illumination.[81] Figure 9a schematically shows the configuration of the later scheme where one can time-gate the illumination. An acousto-optic modulator is employed to gate excitation laser such that the tip and sample are selectively illuminated only for a certain tip−sample separation. Figure 9b shows the sinusoidal oscillation of the tip and the synchronized opening of the time-gate. By selecting a particular value of the time delay (τ) of the time gate, one can select any desired tip−sample separation. The accuracy in the tip−sample separation is determined from the gate-width Δ. TERS spectra corresponding to a desired tip−sample separation can be recorded with high accuracy. By sweeping the value of τ, one can obtain a tip−sample-separation-dependent data set of TERS spectra.

Since the tip apex in TERS measurement is excited by a propagating light, the near-field signal is always accompanied by a far-field propagating light. Therefore, the near-field TERS signal is always combined with a far-field Raman scattering originating from the propagating light, which constitutes a far-field background in TERS.[155,173] For weakly enhanced samples, the enhanced signal can be buried in the far-field background, and thus the usual TERS technique may not be suitable for such samples. Pure near-field Raman signal in TERS can only be obtained by subtracting this far-field background, which is usually done by measuring Raman images twice: once by bringing a metallic nanotip close to the sample and once by retracting the tip away from the sample. In this method, while one can get pure near-field image, it is time-consuming as well as there is a possibility of spatial shift between the two images, which can result in poor quality of the subtracted image. On the other hand, one can simultaneously measure both far- and near-field signals by opening two suitable time gates during the oscillation of the tip. One gate would correspond to the situation when the tip is on the sample, and the other gate would coincide with the situation when tip is far from the sample. Raman signal can be measured through both time gates in each oscillation cycle at every scanning point. In this way, one can perform dynamic in situ far-field background removal

DOI: 10.1021/acs.chemrev.6b00821
Chem. Rev. 2017, 117, 6447−6466

during the imaging process and obtain a pure near-field TERS image.[82]

Apart from dynamic background removal, as mentioned earlier, one can also study different kind of tip−sample interactions individually by precisely controlling the position of the time gate. For example, when the tip is retracted away from the sample by a few tens of nanometers, the EM interaction would start to lose its significance. On the other hand, if the tip−sample separation is less than a nanometer, the metal atoms on the tip apex can chemically interact with the sample molecules and a strong chemical effect can be observed in TERS measurement. Similarly, if the tip applies a pressure on the sample, or in other words, when the tip−sample separation takes a negative value, sample can be locally and temporarily distorted by the tip-applied force and a significant mechanical effect starts to play a role in TERS. These three coexisting effects can be distinctly separated in TERS if one can control the tip−sample separation at subnanometer precision.

In an interesting work, the authors have demonstrated how the three tip−sample interactions can be individually observed in one experiment.[81] A self-assembled adenine nanocrystal with the size of about 80 × 80 × 7 nm^3 was used to demonstrate the tip−sample separation control with high accuracy. Adenine has a strong affinity to silver,and it therefore shows strong chemical effects in Raman scattering.[174] Adenine nanocrystal also shows spectral shift when compressed by the tip, making it easier to see spectral change due to mechanical interaction. Figure 9c shows the TERS spectra measured from the adenine sample at different tip−sample separation by properly controlling the time gate. The inset on the right illustrates the tip−sample separation for each spectrum. In this experiment, the temporal width of the time-gate was set to 0.2 μs, which was about 1/40 of the tapping period (8.0 μs) of the cantilever. The maximum tip-applied force on the sample was set to about 0.4 nN. The authors calculated that the sample was compressed by 1.0 nm under this tip-applied force. The tip−sample separation, *d*, was measured from the upper surface of the sample, hence *d* takes a negative value when the sample is compressed under tip-applied pressure. The spectra shown in Figure 9c are in the spectral range of the ring-breathing mode (RBM) of adenine, with a prominent peak at about 721 cm^{-1}. The spectrum taken for the maximum tip−sample separation (far-field) shows only one peak. The other spectra, which were measured when the tip was in the close vicinity of the sample, show an additional peak (shown in red) that shifts depending upon the tip−sample interaction. As the tip came near the sample at a separation of 0.1 nm, some adenine molecules of the sample started to chemically interact with silver atoms on the tip. This chemical interaction shifted the RBM mode by 10 cm^{-1}, and it appeared at 731 cm^{-1} as a new peak. When the tip−sample separation was further reduced to zero, more adenine molecules came under chemical interaction, resulting in increase in the intensity of the new peak. Finally, when the tip-applied force was increased to 0.4 nN, adenine nanocrystal was compressed with a negative valued of the tip−sample separation and the red peak went under significant changes in both frequency and intensity. These drastic changes are due to an additional effect of mechanical interaction. The peak further shifted by 5 cm^{-1} to appear at 736 cm^{-1}. The increase in intensity can be attributed to the increased number of adenine molecules in contact with the tip. Thus, one can see from Figure 9c that the three effects clearly show up when the tip−sample separation is precisely controlled. This technological improvement in TERS is extremely interesting and useful, as it can address some critical issues at a very precise tip−sample separation control of angstrom level.

6.3. Mechanical Effects in TERS

The mechanical interaction between tip and sample in TERS can bring in some very interesting results; one of them is about achieving much higher resolution than in usual TERS. When the probe tip comes in contact with the sample molecules during TERS experiments, it can apply localized force or pressure on those sample molecules that are directly in contact with the tip. Since the contact area depends on the amount of pressure applied by the tip, it can be much smaller than the size of the confined field at the tip apex. The sample molecules which are pushed by the tip apex can be deformed and hence have a perturbed vibrational response, which can affect the TERS spectrum.[116,175] In general, this tip-applied pressure is unavoidable and uncontrollable in TERS experiments. However, with a precise control over the tip-applied pressure, it can be utilized to benefit the spatial resolution in TERS measurements. This is because the localized deformation of sample molecules can show up in Raman spectral changes such as peak-shift and intensity variation, and address the nanomechanical and nanoelectronic properties of the deformed sample. By precisely controlling the tip-applied force, it is even possible to make sure that a single or a very few molecules of the sample undergo a mechanical perturbation. By sensing the modified TERS response of these few sample molecules, one can potentially achieve a resolution as high as of molecular level. The effect of tip-applied pressure in TERS can be found in literature for several samples, such as C-60, SWNT, and adenine molecules.[116,175] Yano et al. have demonstrated high spatial resolution in TERS where they utilized the tip-applied pressure to achieve the same for SWNT.[162]

Figure 10a shows some TERS spectra of an isolated semiconducting SWNT in the G-mode spectral region, taken under different tip-applied forces, which are indicated in the figure. An isolated SWNT can be locally deformed under this tip-applied force, as illustrated in Figure 10b. One can notice that TERS spectra can be deconvoluted into two peaks at increased values of the tip-applied forces. The new peak, indicated by red dotted line (ω_1), shows up when the tip-applied force is about 1.5 nN and shifts by about 10 cm^{-1} as the tip-applied force increases to 2.4 nN. This new peak is the perturbed G-mode originating from the deformed part of the SWNT. The other peak, indicated by blue dashed line (ω_0), relates to the part of the SWNT that is unpressurized but still falls within the confined light at the tip apex. This peak remains at its original position as it is unaffected by the tip-applied force. The large shift of 10 cm^{-1} confirms that it is easily possible to distinguish the pressurized part of the SWNT, even when the amount of compression is very little, under a tip-applied force of about 2.4 nN.

Figure 10c shows a 3D AFM image of an isolated SWNT, overlaid with illustration of a tip that is scanned over the SWNT along the white dotted line under a constant tip-applied pressure of 2.4 nN. The spectral changes initiating from the tip-applied pressure are relatively more localized than that due to the plasmonic enhancement. Therefore, a nanoimaging based on tip-pressurized TERS has a potential to achieve much better spatial resolution compared to the normal TERS. While the major spectral change due to the plasmonic effects is high enhancement in Raman scattering, the tip-applied pressure

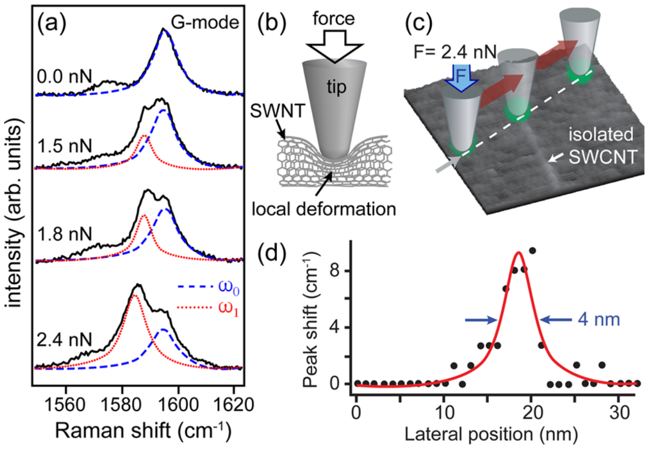

Figure 10. (a) TERS spectra of an isolated SWNT in the G-mode spectral range at indicated tip-applied forces. The deconvoluted spectra show that a new peak (shown in red) starts to appear and shifts as the tip-applied force increases. This new peak corresponds to the perturbed G-mode that originates from the pressurized volume of the sample. The original peak (shown in red) originated from the unpressurized volume of the sample, remains at its initial position. (b) An illustration of local deformation of an isolated SWNT under tip-applied force. (c) AFM image of an isolated SWNT, overlaid with an illustration of tip scanning across the SWNT along the white dotted line with a tip-applied force of 2.4 nN. (d) Shift of the G-mode peak as a function of the lateral position of the tip during the line scan. The shift is largest when the tip is exactly above the SWNT. The best fitting curve shows a spatial resolution of 4 nm in this one-dimensional imaging. Reproduced with permission from ref 162. Copyright 2009 NPG.

predominantly induces shifts in Raman modes. Therefore, unlike normal TERS imaging, tip-pressurized TERS imaging is performed by sensing the amount of peak shift. Figure 10d shows the result of a one-dimensional imaging of the isolated SWNT shown in Figure 10c, where the peak-shift of the G-mode is plotted with respect to the tip position.[162] The peak-shift was measured at the intervals of 1 nm, as the tip was raster scanned across the SWNT. The experimental data are shown by the full circles and the best fitting to the experimental data is shown by the red curve. The spatial resolution obtained from the fwhm of fitting curve in Figure 10d is 4 nm. Similar special resolution was also demonstrated for adenine sample.[162] This is an extremely high value of spatial resolution that the authors demonstrated by combining the mechanical effect of tip-applied pressure with the plasmonic effect of TERS microscopy.

Apart from the extremely high spatial resolution in TERS imaging, the inclusion of such a mechanical effect in TERS also has other benefits in understanding some basic physical and electronic properties of a sample, and thus making practical usage of those properties. For example, when locally pressurized, the electronic band gap of a sample can change within a nanometric volume, which can show up in the variation of Raman intensity in a TERS spectrum. Therefore, tip-pressurized TERS has a potential to provide a new insight into the band gap engineering at nano scale. In another example, one can see in situ phase transition of a SWNT from semiconducting to metallic and vise-versa.[176] Obviously, this technique is not limited only to SWNT, and one can imagine several other useful applications of tip-applied pressure combined with the enhancement of TERS.

7. SUMMARY AND OUTLOOK

In this review, we have discussed the diffraction limit that prevents us from obtaining nano scale resolution in optical imaging. It is, nevertheless, possible to overcome this diffraction limit if the evanescent component of light is involved in the imaging process. This has been shown with plasmonics-based TERS microscopy, where it was demonstrated that TERS can achieve a high spatial resolution, far beyond the diffraction limit, much smaller than the wavelength of the probing light. A spatial resolution as high as 10−15 nm has been achieved by several groups. The inclusion of mechanical interaction has been shown to further improve the spatial resolution down to 3−4 nm. In the recent years, a few groups have claimed to obtain molecular or even submolecular resolution in TERS imaging. This is a remarkable value of spatial resolution one could obtain in any optical imaging. In addition to the high spatial resolution, other benefits of plasmonic, chemical, and mechanical interactions have been realized at the nanoscale. This technique is slowly becoming more popular as new research groups are getting involved and demonstrating further refinement and improvement in the technique with several new and interesting applications. For example, recent TERS imaging experiments have demonstrated the capability of obtaining spatially resolved chemical information, which may lead to answer some important scientific questions about the chemical, physical, and biological properties of a sample. The recently demonstrated utilization of ultrafast pulses in TERS may lead to probing the nonlinear response at the nanoscale and will provide site-specific information about the dynamics of the molecular system.[177] As TERS progresses to establish itself as a tool for nanoinvestigation, it is likely to play an important role in the characterization of electronic and optoelectronic devices, because these devices are now shrinking to nanometer size.

Even after this impressive development of TERS over the years, there are still some important shortcomings remaining today, which we hope would find some practical solutions in the coming years. One of the biggest issues in TERS, which got noticed a lot, is the low controllability of the surface morphology and the reproducibility of the tips. Although the success rate of producing good tips with strong enhancement has increased from about 30% to almost 100%,[77,178] it is still not possible to grow two identical tips with same surface morphologies. Therefore, even after reproducing strong enhancement, some other phenomena, such as the polarization of the near-field light, cannot be well controlled or reproduced. Good reproducibility and mass production of tips would help TERS become a standard tool for nanoscale analysis of various materials, which is still challenging.

Due to the inherent weak nature of Raman scattering, one of the noticeable disadvantages of TERS imaging is the sensitivity or the contrast in comparison with other optical methods, such as the conventional SNOM, which involves relatively stronger Rayleigh scattering,[179] or the newly emerging nano-IR imaging,[180] which is based on IR absorption.

Although TERS and nano-IR can be considered as complementary techniques with different strengths, nano-IR has an advantage that it can directly detect light absorbed by the sample to sense the absorption coefficient via thermal expansion and hence can image optical properties of the sample with better sensitivity. Particularly, it excels for soft matter studies because these materials usually have high thermal expansion.

DOI: 10.1021/acs.chemrev.6b00821
Chem. Rev. 2017, 117, 6447−6466

Another issue that has hindered the acceptance of TERS as a regular tool for nanoscale investigation is the strong inherent far-field scattering background originating from the diffraction-limited focus spot, as it drastically deteriorates the contrast in TERS images. In order to overcome this problem, two techniques have been suggested. One utilizes the so-called plasmon nanofocusing, where the light is coupled to the surface plasmons of the tip at a location far from the tip apex, so that the focus spot and the near-field light are physically separated and hence the background scattering is eliminated.[113−115] The other technique is based on in situ removal of the far-field background by utilizing time-gated tapping mode operation of AFM controller.[82] Both these methods are highly technical and need special skill. It remains interesting to see if there are easier solutions to get rid of the far-field background in TERS imaging, which will help efficient nanoimaging of samples with small Raman cross sections, such as biosamples.

Since TERS involves highly confined light field near the apex of the probe tip, one disadvantage of TERS is that it cannot measure a sample three dimensionally, and remains as a surface technique so far. It will be interesting to see if some researchers come up with an idea to effectively image the intrinsic properties of a sample three dimensionally at nanoscale using TERS.

As mentioned before, molecular and submolecular spatial resolution in TERS imaging have been experimentally demonstrated. The mechanism and the physics behind such super resolution is still under debate and is not fully understood yet. Further research is required to solve the mystery of such a high spatial resolution, which cannot be explained by the existing knowledge of the confinement mechanism.

It is more than one and a half decades since TERS was first demonstrated. Within this short period, TERS has continuously evolved and matured with impressive applications in various fields. Even though there are still many challenges and debatable underlying science behind the unexpectedly high spatial resolution, TERS has already been recognized as one of the best and strongest techniques to optically study a sample at nanoscale. It will be interesting to see the direction of upcoming research in TERS and its new and interesting applications in the future.

ASSOCIATED CONTENT

Special Issue Paper

This paper is an additional review for *Chem. Rev.* **2014**, *117*, issue 7, "Vibrational Nanoscopy".

AUTHOR INFORMATION

Corresponding Author

*E-mail: verma@ap.eng.osaka-u.ac.jp.

ORCID

Prabhat Verma: 0000-0002-7781-418X

Notes

The author declares no competing financial interest.

Biography

Prabhat Verma is a Professor at the Department of Applied Physics and a member of the Photonics Center at Osaka University in Japan, where he leads a research team on Nanospectroscopy. He is also an Executive Director of the Japan Society of Applied Physics and the Chair of the JSPS Core-to-Core Program at Osaka University. He received his Master from IIT Kanpur and Doctorate from IIT Delhi, both in India, after which he went for postdoctoral research in Germany and in Japan. He joined Osaka University in 2002 as an Associate Professor and subsequently became a full Professor in 2010. Prof. Verma is one of the world leaders in the field of tip-enhanced Raman spectroscopy (TERS). His current research interest includes plasmonics, nanospectroscopy, and nanoimaging.

REFERENCES

(1) Fleischmann, M.; Hendra, P. J.; McQuillan, A. Raman Spectra of Pyridine Adsorbed at a Silver Electrode. *Chem. Phys. Lett.* **1974**, *26*, 163−166.

(2) Albrecht, M. G.; Creighton, J. A. Anomalously Intense Raman Spectra of Pyridine at a Silver Electrode. *J. Am. Chem. Soc.* **1977**, *99*, 5215−5217.

(3) Jeanmaire, D. L.; Vanduyne, R. P. Surface Raman Spectroelectrochemistry: Part I. Heterocyclic, Aromatic, and Aliphatic Amines Adsorbed on the Anodized Silver Electrode. *J. Electroanal. Chem. Interfacial Electrochem.* **1977**, *84*, 1−20.

(4) Metiu, H.; Das, P. The Electromagnetic Theory of Surface Enhanced Spectroscopy. *Annu. Rev. Phys. Chem.* **1984**, *35*, 507−536.

(5) Xu, H. X.; Bjerneld, E. J.; Kall, M.; Borjesson, L. Spectroscopy of Single Hemoglobin Molecules by Surface Enhanced Raman Scattering. *Phys. Rev. Lett.* **1999**, *83*, 4357−4360.

(6) Moskovits, M. Surface-Enhanced Spectroscopy. *Rev. Mod. Phys.* **1985**, *57*, 783−826.

(7) Osawa, M.; Matsuda, N.; Yoshii, K.; Uchida, I. Charge Transfer Resonance Raman Process in Surface-Enhanced Raman Scattering from p-aminothiophenol Adsorbed on Silver: Herzberg-Teller Contribution. *J. Phys. Chem.* **1994**, *98*, 12702−12707.

(8) Otto, A.; Mrozek, I.; Grabhorn, H.; Akemann, W. Surface-Enhanced Raman Scattering. *J. Phys.: Condens. Matter* **1992**, *4*, 1143−1212.

(9) Nie, S. M.; Emory, S. R. Probing Single Molecules and Single Nanoparticles by Surface-Enhanced Raman Scattering. *Science* **1997**, *275*, 1102−1106.

(10) Kneipp, K.; Wang, Y.; Kneipp, H.; Perelman, L. T.; Itzkan, I.; Dasari, R.; Feld, M. S. Single Molecule Detection Using Surface-Enhanced Raman Scattering (SERS). *Phys. Rev. Lett.* **1997**, *78*, 1667−1670.

(11) Lim, D. K.; Jeon, K. S.; Kim, H. M.; Nam, J. M.; Suh, Y. D. Nanogap-Engineerable Raman-Active Nanodumbbells for Single-Molecule Detection. *Nat. Mater.* **2010**, *9*, 60−67.

(12) Wang, D. X.; Zhu, W. Q.; Best, M. D.; Camden, J. P.; Crozier, K. B. Directional Raman Scattering from Single Molecules in the Feed Gaps of Optical Antennas. *Nano Lett.* **2013**, *13*, 2194−2198.

(13) Xia, L.; Chen, M.; Zhao, X.; Zhang, Z.; Xia, J.; Xu, H.; Sun, M. T. Visualized Method of Chemical Enhancement Mechanism on SERS and TERS. *J. Raman Spectrosc.* **2014**, *45*, 533−540.

(14) Kneipp, K.; Kneipp, H.; Kartha, B.; Manoharan, R.; Deinum, G.; Itzkan, I.; Dasari, R. R.; Feld, M. S. Detection and Identification of a Single DNA Base Molecule Using Surface-Enhanced Raman Scattering (SERS). *Phys. Rev. E: Stat. Phys., Plasmas, Fluids, Relat. Interdiscip. Top.* **1998**, *57*, R6281−R6284.

(15) Shafer-Peltier, K. E.; Haynes, C. L.; Glucksberg, M. R.; Van Duyne, R. P. Toward a Glucose Biosensor Based on Surface-Enhanced Raman Scattering. *J. Am. Chem. Soc.* **2003**, *125*, 588−593.

(16) Doering, W. E.; Nie, S. M. Single-Molecule and Single-Nanoparticle SERS: Examining the Roles of Surface Active Sites and Chemical Enhancement. *J. Phys. Chem. B* **2002**, *106*, 311−317.

(17) Zhang, X.; Young, M. A.; Lyandres, O.; Van Duyne, R. P. Rapid Detection of an Anthrax Biomarker by Surface-Enhanced Raman Spectroscopy. *J. Am. Chem. Soc.* **2005**, *127*, 4484−4489.

(18) Weiss, A.; Haran, G. Time-Dependent Single-Molecule Raman Scattering as a Probe of Surface Dynamics. *J. Phys. Chem. B* **2001**, *105*, 12348−12354.

(19) Zhou, Q.; Fan, Q.; Zhuang, Y.; Li, Y.; Zhao, G.; Zheng, J. Effect of Substrate on Surface-Enhanced Raman Scattering of Molecules

Adsorbed on Immobilized Silver Nanoparticles. *J. Phys. Chem. B* **2006**, *110*, 12029−12033.

(20) Campion, A.; Kambhampati, P. Surface-Enhanced Raman Scattering. *Chem. Soc. Rev.* **1998**, *27*, 241−250.

(21) Kudelski, A.; Pettinger, B. SERS on Carbon Chain Segments: Monitoring Locally Surface Chemistry. *Chem. Phys. Lett.* **2000**, *321*, 356−362.

(22) Zhang, W. H.; Cui, X. D.; Yeo, B. S.; Schmid, T.; Hafner, C.; Zenobi, R. Nanoscale Roughness on Metal Surfaces Can Increase Tip-Enhanced Raman Scattering by an Order of Magnitude. *Nano Lett.* **2007**, *7*, 1401−1405.

(23) Etchegoin, P. G.; Lacharmoise, P. D.; Le Ru, E. C. Influence of Photostability on Single-Molecule Surface Enhanced Raman Scattering Enhancement Factors. *Anal. Chem.* **2009**, *81*, 682−688.

(24) Freeman, R. G.; Grabar, K. C.; Allison, K. J.; Bright, R. M.; Davis, J. A.; Guthrie, A. P.; Hommer, M. B.; Jackson, M. A.; Smith, P. C.; Walter, D. G.; Natan, M. J. Self-Assembled Metal Colloid Monolayers: An Approach to SERS Substrates. *Science* **1995**, *267*, 1629−1632.

(25) Douketis, C.; Wang, Z.; Haslett, T. L.; Moskovits, M. Fractal Character of Cold-Deposited Silver Films Determined by Low-Temperature Scanning Tunneling Microscopy. *Phys. Rev. B: Condens. Matter Mater. Phys.* **1995**, *51*, 11022.

(26) Hu, X.; Wang, T.; Wang, L.; Dong, S. Surface-Enhanced Raman Scattering of 4-Aminothiophenol Self-Assembled Monolayers in Sandwich Structure with Nanoparticle Shape Dependence: Off-Surface Plasmon Resonance Condition. *J. Phys. Chem. C* **2007**, *111*, 6962−6969.

(27) Jackson, J. B.; Halas, N. J. Surface-Enhanced Raman Scattering on Tunable Plasmonic Nanoparticle Substrates. *Proc. Natl. Acad. Sci. U. S. A.* **2004**, *101*, 17930.

(28) Kawata, S.; Inouye, Y.; Verma, P. Plasmonics for Near-Field Nano-Imaging and Superlensing. *Nat. Photonics* **2009**, *3*, 388−394.

(29) Zhao, L. L.; Jensen, L.; Schatz, G. C. Surface-Enhanced Raman Scattering of Pyrazine at the Junction between Two Ag_{20} Nanoclusters. *Nano Lett.* **2006**, *6*, 1229−1234.

(30) Nikoobakht, B.; Wang, J.; El-Sayed, M. A. Surface-Enhanced Raman Scattering of Molecules Adsorbed on Gold Nanorods: Off-Surface Plasmon Resonance Condition. *Chem. Phys. Lett.* **2002**, *366*, 17−23.

(31) Hao, E.; Schatz, G. C. Electromagnetic Fields Around Silver Nanoparticles and Dimers. *J. Chem. Phys.* **2004**, *120*, 357−366.

(32) Fromm, D. P.; Sundaramurthy, A.; Schuck, J.; Kino, G.; Moerner, W. E. Gap-Dependent Optical Coupling of Single "Bowtie" Nanoantennas Resonant in the Visible. *Nano Lett.* **2004**, *4*, 957−961.

(33) Jensen, L.; Aikens, C. M.; Schatz, G. C. Electronic structure methods for studying surface-enhanced Raman scattering. *Chem. Soc. Rev.* **2008**, *37*, 1061−1073.

(34) Michaels, A. M.; Jiang, J.; Brus, L. Ag Nanocrystal Junctions as the Site for Surface-Enhanced Raman Scattering of Single Rhodamine 6G Molecules. *J. Phys. Chem. B* **2000**, *104*, 11965−11971.

(35) Xu, H.; Bjerneld, E. J.; Käll, M.; Börjesson, L. Spectroscopy of Single Hemoglobin Molecules by Surface Enhanced Raman Scattering. *Phys. Rev. Lett.* **1999**, *83*, 4357−4360.

(36) Xu, H.; Aizpurua, J.; Kall, M.; Apell, P. Electromagnetic Contributions to Single-Molecule Sensitivity in Surface-Enhanced Raman Scattering. *Phys. Rev. E: Stat. Phys., Plasmas, Fluids, Relat. Interdiscip. Top.* **2000**, *62*, 4318−4324.

(37) Angel, S. M.; Myrick, M. L. Near-Infrared Surface-Enhanced Raman Spectroscopy Using A Diode Laser. *Anal. Chem.* **1989**, *61*, 1648−1652.

(38) Wang, L.-R.; Fang, Y. IR-SERS Study and Theoretical Analogue on the Adsorption Behavior of Pyridine Carboxylic Acid on Silver Nanoparticles. *Spectrochim. Acta, Part A* **2006**, *63*, 614−618.

(39) Ren, B.; Lin, X.-F.; Yang, Z.-L.; Liu, G.-K.; Aroca, R. F.; Mao, B.-W.; Tian, Z.-Q. Surface-Enhanced Raman Scattering in the Ultraviolet Spectral Region: UV-SERS on Rhodium and Ruthenium Electrodes. *J. Am. Chem. Soc.* **2003**, *125*, 9598−9599.

(40) Yang, Z.-L.; Li, Q.-H.; Ren, B.; Tian, Z.-Q. Tunable SERS from Aluminium Nanohole Arrays in the Ultraviolet Region. *Chem. Commun.* **2011**, *47*, 3909−3911.

(41) Dörfer, T.; Schmitt, M.; Popp, J. Deep-UV Surface-Enhanced Raman Scattering. *J. Raman Spectrosc.* **2007**, *38*, 1379−1382.

(42) Ding, T.; Sigle, D. O.; Herrmann, L. O.; Wolverson, D.; Baumberg, J. J. Nanoimprint Lithography of Al Nanovoids for Deep-UV SERS. *ACS Appl. Mater. Interfaces* **2014**, *6*, 17358−17363.

(43) Abbe, E. Beiträge zur Theorie des Mikroskops und der Mikroskopischen Wahrnehmung. *Arch. Mikrosk. Anat.* **1873**, *9*, 413−468.

(44) Rayleigh, L. On the Theory of Optical Images, with Special Reference to the Microscope. *Philos. Mag.* **1896**, *42*, 167−195.

(45) Wessel, J. Surface-Enhanced Optical Microscopy. *J. Opt. Soc. Am. B* **1985**, *2*, 1538−1551.

(46) Synge, E. H. A Suggested Method for Extending Microscopic Resolution into the Ultra-Microscopic Region. *Philos. Mag.* **1928**, *6*, 356−362.

(47) Kawata, S.; Inouye, Y.; Sugiura, T. Near-Field Scanning Optical Microscope with a Laser Trapped Probe. *Jpn. J. Appl. Phys.* **1994**, *33*, L1725−L1727.

(48) Inouye, Y.; Kawata, S. Near-field Scanning Optical Microscope using a Metallic Probe Tip. *Opt. Lett.* **1994**, *19*, 159−161.

(49) Inouye, Y.; Hayazawa, N.; Hayashi, K.; Sekkat, Z.; Kawata, S. Near-Field Scanning Optical Microscope using a Metallized Cantilever Tip for Nanospectroscopy. *Proc. SPIE* **1999**, *3791*, 40−48.

(50) Stockle, R. M.; Suh, Y. D.; Deckert, V.; Zenobi, R. Nanoscale Chemical Analysis by Tip-Enhanced Raman Spectroscopy. *Chem. Phys. Lett.* **2000**, *318*, 131−136.

(51) Hayazawa, N.; Inouye, Y.; Sekkat, Z.; Kawata, S. Metallized Tip Amplification of Near-Field Raman Scattering. *Opt. Commun.* **2000**, *183*, 333−336.

(52) Anderson, M. S. Locally Enhanced Raman Spectroscopy with an Atomic Force Microscope. *Appl. Phys. Lett.* **2000**, *76*, 3130−3132.

(53) Pettinger, B.; Picardi, G.; Schuster, R.; Ertl, G. Surface Enhanced Raman Spectroscopy: Towards Single Moleculer Spectroscopy. *Electrochemistry* **2000**, *68*, 942−949.

(54) Binnig, G.; Rohrer, H.; Gerber, Ch.; Weibel, E. Surface Studies by Scanning Tunneling Microscopy. *Phys. Rev. Lett.* **1982**, *49*, 57−61.

(55) Binnig, G.; Rohrer, H.; Gerber, Ch. Atomic Force Microscope. *Phys. Rev. Lett.* **1986**, *56*, 930−933.

(56) Suh, Y. D.; Soeckle, R. M.; Deckert, V.; Zenobi, R. Tip-Enhanced Raman Spectroscopy as a New Analytical Tool for Nanomaterials. *Abstr. Pap. Am. Chem. Soc.* **2001**, *221*, U91.

(57) Pettinger, B.; Picardi, G.; Schuster, R.; Ertl, G. Surface-Enhanced and STM-Tip-Enhanced Raman Spectroscopy at Metal Surfaces. *Single Mol.* **2002**, *3*, 285−294.

(58) Deckert, V. Tip-Enhanced Raman Spectroscopy. *J. Raman Spectrosc.* **2009**, *40*, 1336−1337.

(59) Domke, K. F.; Pettinger, B. Studying Surface Chemistry beyond the Diffraction Limit: 10 Years of TERS. *ChemPhysChem* **2010**, *11*, 1365−1373.

(60) Kim, T.; Jeon, K.; Heo, K.; Kim, H. M.; Park, J.; Suh, Y. D.; Hong, S. Multilayered Nano-Prism Vertex Tips for Tip-Enhanced Raman Spectroscopy and Imaging. *Analyst* **2013**, *138*, 5588−5593.

(61) Schmid, T.; Opilik, L.; Blum, C.; Zenobi, R. Nanoscale Chemical Imaging Using Tip-Enhanced Raman Spectroscopy: A Critical Review. *Angew. Chem., Int. Ed.* **2013**, *52*, 5940−5954.

(62) Sonntag, M. D.; Pozzi, E. A.; Jiang, N.; Hersam, M. C.; Van Duyne, R. P. Recent Advances in Tip-Enhanced Raman Spectroscopy. *J. Phys. Chem. Lett.* **2014**, *5*, 3125−3130.

(63) Blum, C.; Opilik, L.; Atkin, J. M.; Braun, K.; Kämmer, S. B.; Kravtsov, V.; Kumar, N.; Lemeshko, S.; Li, J.-F.; Luszcz, K.; et al. Tip-Enhanced Raman Spectroscopy - an Interlaboratory Reproducibility and Comparison Study. *J. Raman Spectrosc.* **2014**, *45*, 22−31.

(64) Langelüddecke, L.; Singh, P.; Deckert, V. Exploring the Nanoscale: Fifteen Years of Tip- Enhanced Raman Spectroscopy. *Appl. Spectrosc.* **2015**, *69*, 1357−1371.

(65) Kumar, N.; Mignuzzi, S.; Su, W.; Roy, D. Tip-Enhanced Raman Spectroscopy: Principles and Applications. *EPJ. Technol. Instrum.* **2015**, *2*, 9.

(66) Fujita, Y.; Walke, P.; De Feyter, S.; Uji-I, H. Tip-Enhanced Raman Scattering Microscopy: Recent Advance in Tip Production. *Jpn. J. Appl. Phys.* **2016**, *55*, 08NA02.

(67) Su, W.; Kumar, N.; Dai, N.; Roy, D. Nanoscale Mapping of Intrinsic Defects in Single-Layer Graphene Using Tip-Enhanced Raman Spectroscopy. *Chem. Commun.* **2016**, *52*, 8227−8230.

(68) Zrimsek, A. B.; Chiang, N.; Mattei, M.; Zaleski, S.; McAnally, M. O.; Chapman, C. T.; Henry, A.-I.; Schatz, G. C.; Van Duyne, R. P. Single-Molecule Chemistry with Surface- and Tip-Enhanced Raman Spectroscopy. *Chem. Rev.* **2016**, DOI: 10.1021/acs.chemrev.6b00552.

(69) Park, K.-D.; Raschke, M. B.; Atkin, J. M.; Lee, Y. H.; Jeong, M. S. Probing Bilayer Grain Boundaries in Large-Area Graphene with Tip-Enhanced Raman Spectroscopy. *Adv. Mater.* **2017**, *29*, 1603601.

(70) Otto, A. Excitation of Nonradiative Surface Plasma Waves in Silver by the Method of Frustrated Total Reflection. *Z. Phys. A: Hadrons Nucl.* **1968**, *216*, 398−410.

(71) Otto, A. Eine Neue Methode der Anregung Nichtstrahlender Oberflächenplasmaschwingungen. *Phys. Status Solidi B* **1968**, *26*, K99−K101.

(72) Kretschmann, E.; Raether, H. Radiative Decay of Non Radiative Surface Plasmons Excited by Light. *Z. Naturforsch., A: Phys. Sci.* **1968**, *23*, 2135−2136.

(73) Saito, S.; Ohashi, Y.; Verma, P. Optimization of s-Polarization Sensitivity in Apertureless Near-Field Optical Microscopy. *Int. J. Opt.* **2012**, *2012*, 1−6.

(74) Saito, S.; Verma, P. Polarization-Controlled Raman Microscopy and Nanoscopy. *J. Phys. Chem. Lett.* **2012**, *3*, 1295−1300.

(75) Klingsporn, J. M.; Jiang, N.; Pozzi, E. A.; Sonntag, M. D.; Chulhai, D.; Seideman, T.; Jensen, L.; Hersam, M. C.; Van Duyne, R. P. Intramolecular Insight into Adsorbate−Substrate Interactions via Low-Temperature, Ultrahigh-Vacuum Tip-Enhanced Raman Spectroscopy. *J. Am. Chem. Soc.* **2014**, *136*, 3881−3887.

(76) Zhang, D.; Wang, X.; Braun, K.; Egelhaaf, H.-J.; Fleischer, M.; Hennemann, L.; Hintz, H.; Stanciu, C.; Brabec, C. J.; Kern, D. P.; Meixner, A. J. Parabolic Mirror-Assisted Tip-Enhanced Spectroscopic Imaging for Non-Transparent Materials. *J. Raman Spectrosc.* **2009**, *40*, 1371−1376.

(77) Yeo, B.-S.; Schmid, T.; Zhang, W.; Zenobi, R. Towards Rapid Nanoscale Chemical Analysis Using Tip-Enhanced Raman Spectroscopy with Ag-Coated Dielectric Tips. *Anal. Bioanal. Chem.* **2007**, *387*, 2655−2662.

(78) Saito, Y.; Wang, J. J.; Smith, D. A.; Batchelder, D. N. A Simple Chemical Method for the Preparation of Silver Surfaces for Efficient SERS. *Langmuir* **2002**, *18*, 2959−2961.

(79) Hayazawa, N.; Inouye, Y.; Sekkat, Z.; Kawata, S. Near-Field Raman Scattering Enhanced by a Metallized Tip. *Chem. Phys. Lett.* **2001**, *335*, 369−374.

(80) Saito, Y.; Hayazawa, N.; Kataura, H.; Murakami, T.; Tsukagoshi, K.; Inouye, Y.; Kawata, S. Polarization Measurements in Tip-Enhanced Raman Spectroscopy Applied to Single-Walled Carbon Nanotubes. *Chem. Phys. Lett.* **2005**, *410*, 136−141.

(81) Ichimura, T.; Fujii, S.; Verma, P.; Yano, T.; Inouye, Y.; Kawata, S. Subnanometric Near-Field Raman Investigation in the Vicinity of a Metallic Nanostructure. *Phys. Rev. Lett.* **2009**, *102*, 186101.

(82) Yu, J.; Saito, Y.; Ichimura, T.; Kawata, S.; Verma, P. Far-Field Free Tapping-Mode Tip-Enhanced Raman Microscopy. *Appl. Phys. Lett.* **2013**, *102*, 123110.

(83) Hartschuh, A.; Sánchez, E. J.; Xie, X. S.; Novotny, L. High-Resolution Near-Field Raman Microscopy of Single-Walled Carbon Nanotubes. *Phys. Rev. Lett.* **2003**, *90*, 095503.

(84) Pettinger, B.; Domke, K. F.; Zhang, D.; Schuster, R.; Ertl, G. Direct monitoring of plasmon resonances in a tip-surface gap of varying width. *Phys. Rev. B: Condens. Matter Mater. Phys.* **2007**, *76*, 113409.

(85) Pettinger, B.; Domke, K. F.; Zhang, D.; Picardi, G.; Schuster, R. Tip-Enhanced Raman Scattering: Influence of the Tip-Surface Geometry on Optical Resonance and Enhancement. *Surf. Sci.* **2009**, *603*, 1335−1341.

(86) Raschke, M. B.; Lienau, C. Apertureless Near-Field Optical Microscopy: Tip−Sample Coupling in Elastic Light Scattering. *Appl. Phys. Lett.* **2003**, *83*, 5089−5091.

(87) Yang, Z.; Aizpurua, J.; Xu, H. Electromagnetic Field Enhancement in TERS Configurations. *J. Raman Spectrosc.* **2009**, *40*, 1343−1348.

(88) Schmid, T.; Yeo, B.-S.; Leong, G.; Stadler, J.; Zenobi, R. Performing Tip-Enhanced Raman Spectroscopy in Liquids. *J. Raman Spectrosc.* **2009**, *40*, 1392−1399.

(89) Yeo, B.-S.; Stadler, J.; Schmid, T.; Zenobi, R.; Zhang, W. H. Tip-Enhanced Raman Spectroscopy - Its Status, Challenges and Future Directions. *Chem. Phys. Lett.* **2009**, *472*, 1−13.

(90) Nakata, A.; Nomoto, T.; Toyota, T.; Fujinami, M. Tip-enhanced Raman Spectroscopy of Lipid Bilayers in Water with an Alumina- and Silver-coated Tungsten Tip. *Anal. Sci.* **2013**, *29*, 865−869.

(91) Touzalin, T.; Dauphin, A. L.; Joiret, S.; Lucas, I. T.; Maisonhaute, E. Tip-Enhanced Raman Spectroscopy Imaging of Opaque Samples in Organic Liquid. *Phys. Chem. Chem. Phys.* **2016**, *18*, 15510−15513.

(92) Kurouski, D.; Mattei, M.; Van Duyne, R. P. Probing Redox Reactions at the Nanoscale with Electrochemical Tip-Enhanced Raman Spectroscopy. *Nano Lett.* **2015**, *15*, 7956−7962.

(93) Zeng, Z.-C.; Huang, S.-C.; Wu, D.-Y.; Meng, L.-Y.; Li, M.-H.; Huang, T.-X.; Zhong, J.-H.; Wang, X.; Yang, Z.-L.; Ren, B. Electrochemical Tip-Enhanced Raman Spectroscopy. *J. Am. Chem. Soc.* **2015**, *137*, 11928−11931.

(94) Sabanés, N. M.; Driessen, L. M. A.; Domke, K. F. Versatile Side-Illumination Geometry for Tip-Enhanced Raman Spectroscopy at Solid/Liquid Interfaces. *Anal. Chem.* **2016**, *88*, 7108−7114.

(95) Hartschuh, A.; Qian, H.; Meixner, A. J.; Anderson, N.; Novotny, L. Nanoscale Optical Imaging of Single-Walled Carbon Nanotubes. *J. Lumin.* **2006**, *119−120*, 204−208.

(96) Hartschuh, A.; Anderson, N.; Novotny, L. Near-Field Raman Spectroscopy using a Sharp Metal Tip. *J. Microsc.* **2003**, *210*, 234−240.

(97) Anger, P.; Bharadwaj, P.; Novotny, L. Enhancement and Quenching of Single-Molecule Fluorescence. *Phys. Rev. Lett.* **2006**, *96*, 113002.

(98) Kalkbrenner, T.; Ramstein, M.; Mlynek, J.; Sandoghdar, V. A Single Gold Particle as a Probe for Apertureless Scanning Near-Field Optical Microscopy. *J. Microsc.* **2001**, *202*, 72−76.

(99) Zou, Y.; Steinvurzel, P.; Yang, T.; Crozier, K. B. Surface Plasmon Resonances of Optical Antenna Atomic Force Microscope Tips. *Appl. Phys. Lett.* **2009**, *94*, 171107.

(100) Nishi, M.; Teranishi, D.; Itasaka, H.; Shimizu, M.; Hirao, K. Silver Growth on AFM Tip Apexes from Silver Nitrate Solutions Triggered by Focused-Ion-Beam Irradiation. *MRS Advances* **2016**, *1*, 1865−1869.

(101) Li, J.-F.; Li, S.-B.; Anema, J. R.; Yang, Z.-L.; Huang, Y.-F.; Ding, Y.; Wu, Y.-F.; Zhou, X.-S.; Wu, D.-Y.; Ren, B.; Wang, Z.-L.; Tian, Z.-Q. Synthesis and Characterization of Gold Nanoparticles Coated with Ultrathin and Chemically Inert Dielectric Shells for SHINERS Applications. *Appl. Spectrosc.* **2011**, *65*, 620−626.

(102) Taguchi, A.; Hayazawa, N.; Furusawa, K.; Ishitobi, H.; Kawata, S. Deep-UV Tip-Enhanced Raman Scattering. *J. Raman Spectrosc.* **2009**, *40*, 1324−1330.

(103) Taguchi, A.; Hayazawa, N.; Saito, Y.; Ishitobi, H.; Tarun, A.; Kawata, S. Controlling the Plasmon Resonance Wavelength in Metal-Coated Probe using Refractive Index Modification. *Opt. Express* **2009**, *17*, 6509−6518.

(104) Molenda, D.; Colas des Francs, G.; Fischer, U. C.; Rau, N.; Naber, A. High-Resolution Mapping of the Optical Near-Field Components at a Triangular Nano-Aperture. *Opt. Express* **2005**, *13*, 10688−10696.

(105) Bortchagovsky, E. G.; Fischer, U. C. A Tetrahedral Tip as a Probe for Tip-Enhanced Raman Scattering and as a Near-Field Raman Probe. *J. Raman Spectrosc.* **2009**, *40*, 1386−1391.

(106) Lewis, A.; Taha, H.; Strinkovski, A.; Manevitch, A.; Khatchatouriants, A.; Dekhter, R.; Ammann, E. Near-Field Optics: from Subwavelength Illumination to Nanometric Shadowing. *Nat. Biotechnol.* **2003**, *21*, 1378−1386.

(107) Sharma, G.; Deckert-Gaudig, T.; Deckert, V. Tip-Enhanced Raman Scattering—Targeting Structure-Specific Surface Characterization for Biomedical Samples. *Adv. Drug Delivery Rev.* **2015**, *89*, 42−56.

(108) Taguchi, A.; Yu, J.; Verma, P.; Kawata, S. Optical Antennas with Multiple Plasmonic Nanoparticles for Tip-Enhanced Raman Microscopy. *Nanoscale* **2015**, *7*, 17424−17433.

(109) Smolyaninov, I. I.; Davis, C. C.; Elliott, J.; Zayats, A. V. Resolution Enhancement of a Surface Immersion Microscope Near the Plasmon Resonance. *Opt. Lett.* **2005**, *30*, 382−384.

(110) Fleischer, M.; Weber-Bargioni, A.; Altoe, M. V. P.; Schwartzberg, A. M.; Schuck, P. J.; Cabrini, S.; Kern, D. P. Gold Nanocone Near-Field Scanning Optical Microscopy Probes. *ACS Nano* **2011**, *5*, 2570−2579.

(111) Umakoshi, T.; Yano, T.; Saito, Y.; Verma, P. Fabrication of Near-Field Plasmonic Tip by Photoreduction for Strong Enhancement in Tip-Enhanced Raman Spectroscopy. *Appl. Phys. Express* **2012**, *5*, 052001.

(112) Maouli, I.; Taguchi, A.; Saito, Y.; Kawata, S.; Verma, P. Optical Antennas for Tunable Enhancement in Tip-Enhanced Raman Spectroscopy Imaging. *Appl. Phys. Express* **2015**, *8*, 032401.

(113) Stockman, M. I. Nanofocusing of Optical Energy in Tapered Plasmonic Waveguides. *Phys. Rev. Lett.* **2004**, *93*, 137404.

(114) Ropers, C.; Neacsu, C. C.; Elsaesser, T.; Albrecht, M.; Raschke, M. B.; Lienau, C. Grating-Coupling of Surface Plasmons onto Metallic Tips: A Nanoconfined Light Source. *Nano Lett.* **2007**, *7*, 2784−2788.

(115) Umakoshi, T.; Saito, Y.; Verma, P. Highly Efficient Plasmonic Tip Design for Plasmon Nanofocusing in Near-Field Optical Microscopy. *Nanoscale* **2016**, *8*, 5634−5640.

(116) Verma, P.; Yamada, K.; Watanabe, H.; Inouye, Y.; Kawata, S. Near-Field Raman Scattering Investigation of Tip Effects on C60 Molecules. *Phys. Rev. B: Condens. Matter Mater. Phys.* **2006**, *73*, 045416.

(117) Yano, T.; Ichimura, T.; Kuwahara, S.; H'Dhili, F.; Uetsuki, K.; Okuno, Y.; Verma, P.; Kawata, S. Tip-Enhanced Nano-Raman Analytical Imaging of Locally Induced Strain Distribution in Carbon Nanotubes. *Nat. Commun.* **2013**, *4*, 2592.

(118) Yano, T.; Verma, P.; Kawata, S. Diameter-Selective Near-Field Raman Analysis and Imaging of Isolated Carbon Nanotube Bundles. *Appl. Phys. Lett.* **2006**, *88*, 093125.

(119) Schmid, T.; Messmer, A.; Yeo, B.-S.; Zhang, W.; Zenobi, R. Towards Chemical Analysis of Nanostructures in Biofilms II: Tip-Enhanced Raman Spectroscopy of Alginates. *Anal. Bioanal. Chem.* **2008**, *391*, 1907−1916.

(120) Cialla, D.; Deckert-Gaudig, T.; Budich, C.; Laue, M.; Moller, R.; Naumann, D.; Deckert, V.; Popp, J. Raman to the Limit: Tip-Enhanced Raman Spectroscopic Investigations of a Single Tobacco Mosaic Virus. *J. Raman Spectrosc.* **2009**, *40*, 240−243.

(121) Neugebauer, U.; Rosch, P.; Schmitt, M.; Popp, J.; Julien, C.; Rasmussen, A.; Budich, C.; Deckert, V. On the Way to Nanometer-Sized Information of the Bacterial Surface by Tip-Enhanced Raman Spectroscopy. *ChemPhysChem* **2006**, *7*, 1428−1430.

(122) Wood, B. R.; Bailo, E.; Khiavi, M. A.; Tilley, L.; Deed, S.; Deckert-Gaudig, T.; McNaughton, D.; Deckert, V. Tip-Enhanced Raman Scattering (TERS) from Hemozoin Crystals within a Sectioned Erythrocyte. *Nano Lett.* **2011**, *11*, 1868−1873.

(123) Böhme, R.; Cialla, D.; Richter, M.; Rösch, P.; Popp, J.; Deckert, V. Biochemical Imaging Below the Diffraction Limit − Probing Cellular Membrane Related Structures by Tip-Enhanced Raman Spectroscopy (TERS). *J. Biophotonics* **2010**, *3*, 455−461.

(124) Bailo, E.; Deckert, V. Tip-Enhanced Raman Spectroscopy of Single RNA Strands: Towards a Novel Direct-Sequencing Method. *Angew. Chem., Int. Ed.* **2008**, *47*, 1658−1661.

(125) Rasmussen, A.; Deckert, V. Surface- and Tip-Enhanced Raman Scattering of DNA Components. *J. Raman Spectrosc.* **2006**, *37*, 311−317.

(126) Ichimura, T.; Hayazawa, N.; Hashimoto, M.; Inouye, Y.; Kawata, S. Tip-Enhanced Coherent Anti-Stokes Raman Scattering for Vibrational Nanoimaging. *Phys. Rev. Lett.* **2004**, *92*, 220801.

(127) Domke, K. F.; Zhang, D.; Pettinger, B. Tip-Enhanced Raman Spectra of Picomole Quantities of DNA Nucleobases at Au(111). *J. Am. Chem. Soc.* **2007**, *129*, 6708−6709.

(128) Zhang, D.; Domke, K. F.; Pettinger, B. Tip-Enhanced Raman Spectroscopic Studies of the Hydrogen Bonding between Adenine and Thymine Adsorbed on Au (111). *ChemPhysChem* **2010**, *11*, 1662−1665.

(129) Kurouski, D.; Deckert-Gaudig, T.; Deckert, V.; Lednev, I. K. Surface Characterization of Insulin Protofilaments and Fibril Polymorphs using Tip-Enhanced Raman Spectroscopy (TERS). *Biophys. J.* **2014**, *106*, 263−271.

(130) Böhme, R.; Richter, M.; Cialla, D.; Rösch, P.; Deckert, V.; Popp, J. Towards a Specific Characterisation of Components on a Cell Surface—Combined TERS-Investigations of Lipids and Human Cells. *J. Raman Spectrosc.* **2009**, *40*, 1452−1457.

(131) Opilik, L.; Bauer, T.; Schmid, T.; Stadler, J.; Zenobi, R. Nanoscale Chemical Imaging of Segregated Lipid Domains Using Tip-Enhanced Raman Spectroscopy. *Phys. Chem. Chem. Phys.* **2011**, *13*, 9978−9981.

(132) Kumar, N.; Drozdz, M. M.; Jiang, H.; Santos, D. M.; Vaux, D. J. Nanoscale Mapping of Newly-Synthesised Phospholipid Molecules in a Biological Cell Using Tip-Enhanced Raman Spectroscopy. *Chem. Commun.* **2017**, *53*, 2451−2454.

(133) Kumar, N.; Stephanidis, B.; Zenobi, R.; Wain, A. J.; Roy, D. Nanoscale Mapping of Catalytic Activity Using Tip-Enhanced Raman Spectroscopy. *Nanoscale* **2015**, *7*, 7133−7137.

(134) Buurmans, I. L. C.; Weckhuysen, B. M. Heterogeneities of Individual Catalyst Particles in Space and Time as Monitored by Spectroscopy. *Nat. Chem.* **2012**, *4*, 873−886.

(135) Yeo, B. S.; Amstad, E.; Schmid, T.; Stadler, J.; Zenobi, R. Nanoscale Probing of a Polymer-Blend Thin Film with Tip-Enhanced Raman Spectroscopy. *Small* **2009**, *5*, 952−960.

(136) Krebs, F. C.; Norrman, K. Analysis of the Failure Mechanism for a Stable Organic Photovoltaic During 10000 h of Testing. *Prog. Photovoltaics* **2007**, *15*, 697−712.

(137) Lee, N.; Hartschuh, R. D.; Mehtani, D.; Kisliuk, A.; Maguire, J. F.; Green, M.; Foster, M. D.; Sokolov, A. P. High Contrast Scanning Nano-Raman Spectroscopy of Silicon. *J. Raman Spectrosc.* **2007**, *38*, 789−796.

(138) Nguyen, Q.; Ossikovski, R.; Schreiber, J. Contrast Enhancement on Crystalline Silicon in Polarized Reflection Mode Tip-Enhanced Raman Spectroscopy. *Opt. Commun.* **2007**, *274*, 231−235.

(139) Hanafusa, H.; Hirose, N.; Kasamatsu, A.; Mimura, T.; Matsui, T.; Chong, H. M. H.; Mizuta, H.; Suda, Y. Strain Distribution Analysis of Sputter-Formed Strained Si by Tip-enhanced Raman Spectroscopy. *Appl. Phys. Express* **2011**, *4*, 025701.

(140) Wang, X.; Zhang, D.; Braun, K.; Egelhaaf, H. J.; Brabec, C. J.; Meixner, A. J. High-Resolution Spectroscopic Mapping of the Chemical Contrast from Nanometer Domains in P3HT:PCBM Organic Blend Films for Solar-Cell Applications. *Adv. Funct. Mater.* **2010**, *20*, 492−499.

(141) van Schrojenstein Lantman, E. M.; Deckert-Gaudig, T.; Mank, A. J. G.; Deckert, V.; Weckhuysen, B. M. Catalytic Processes Monitored at the Nanoscale with Tip-Enhanced Raman Spectroscopy. *Nat. Nanotechnol.* **2012**, *7*, 583−586.

(142) Xiao, L.; Wang, H.; Schultz, Z. D. Selective Detection of RGD-Integrin Binding in Cancer Cells Using Tip Enhanced Raman Scattering Microscopy. *Anal. Chem.* **2016**, *88*, 6547−6553.

(143) Zhang, W.; Yeo, B. S.; Schmid, T.; Zenobi, R. Single Molecule Tip-Enhanced Raman Spectroscopy with Silver Tips. *J. Phys. Chem. C* **2007**, *111*, 1733−1738.

(144) Opilik, L.; Dogan, Ü.; Li, C.-Y.; Stephanidis, B.; Li, J.-F.; Zenobi, R. Chemical Production of Thin Protective Coatings on

Optical Nanotips for Tip-Enhanced Raman Spectroscopy. *J. Phys. Chem. C* **2016**, *120*, 20828−20832.

(145) Tallarida, N.; Rios, L.; Apkarian, V. A.; Lee, J. Isomerization of One Molecule Observed through Tip-Enhanced Raman Spectroscopy. *Nano Lett.* **2015**, *15*, 6386−6394.

(146) Freedman, K. J.; Crick, C. R.; Albella, P.; Barik, A.; Ivanov, A. P.; Maier, S. A.; Oh, S.-H.; Edel, J. B. On-Demand Surface- and Tip-Enhanced Raman Spectroscopy Using Dielectrophoretic Trapping and Nanopore Sensing. *ACS Photonics* **2016**, *3*, 1036−1044.

(147) Hartman, T.; Wondergem, C. S.; Kumar, N.; van den Berg, A.; Weckhuysen, B. M. Surface- and Tip-Enhanced Raman Spectroscopy in Catalysis. *J. Phys. Chem. Lett.* **2016**, *7*, 1570−1584.

(148) Zaleski, S.; Wilson, A. J.; Mattei, M.; Chen, X.; Goubert, G.; Cardinal, M. F.; Willets, K. A.; van Duyne, R. P. Investigating Nanoscale Electrochemistry with Surface- and Tip- Enhanced Raman Spectroscopy. *Acc. Chem. Res.* **2016**, *49*, 2023−2030.

(149) Sonntag, M. D.; Klingsporn, J. M.; Garibay, L. K.; Roberts, J. M.; Dieringer, J. A.; Seideman, T.; Scheidt, K. A.; Jensen, L.; Schatz, G. C.; van Duyne, R. P. Single-Molecule Tip-Enhanced Raman Spectroscopy. *J. Phys. Chem. C* **2012**, *116*, 478−483.

(150) Wickramasinghe, H. K.; Chaigneau, M.; Yasukuni, R.; Picardi, G.; Ossikovski, R. Billion-Fold Increase in Tip-Enhanced Raman Signal. *ACS Nano* **2014**, *8*, 3421−3426.

(151) Liao, M.; Jiang, S.; Hu, C.; Zhang, R.; Kuang, Y.; Zhu, J.; Zhang, Y.; Dong, Z. Tip-Enhanced Raman Spectroscopic Imaging of Individual Carbon Nanotubes with Subnanometer Resolution. *Nano Lett.* **2016**, *16*, 4040−4046.

(152) Najjar, S.; Talaga, D.; Schué, L.; Coffinier, Y.; Szunerits, S.; Boukherroub, R.; Servant, L.; Rodriguez, V.; Bonhommeau, S. Tip-Enhanced Raman Spectroscopy of Combed Double-Stranded DNA Bundles. *J. Phys. Chem. C* **2014**, *118*, 1174−1181.

(153) Anderson, N.; Hartschuh, A.; Cronin, S.; Novotny, L. Nanoscale Vibrational Analysis of Single-Walled Carbon Nanotubes. *J. Am. Chem. Soc.* **2005**, *127*, 2533−2537.

(154) Hillenbrand, R.; Taubner, T.; Keilmann, F. Phonon-Enhanced Light−Matter Interaction at the Nanometre Scale. *Nature* **2002**, *418*, 159−162.

(155) Cançado, L. G.; Hartschuh, A.; Novotny, L. Tip-Enhanced Raman Spectroscopy of Carbon Nanotubes. *J. Raman Spectrosc.* **2009**, *40*, 1420−1426.

(156) Kurouski, D.; Deckert-Gaudig, T.; Deckert, V.; Lednev, I. K. Structure and Composition of Insulin Fibril Surfaces Probed by TERS. *J. Am. Chem. Soc.* **2012**, *134*, 13323−13329.

(157) Deckert, V.; Deckert-Gaudig, T.; Diegel, M.; Gotz, I.; Langeluddecke, L.; Schneidewind, H.; Sharma, G.; Singh, P.; Singh, P.; Trautmann, S.; Zeisberger, M.; Zhang, Z. Spatial Resolution in Raman Spectroscopy. *Faraday Discuss.* **2015**, *177*, 9−20.

(158) Deckert-Gaudig, T.; Bailo, E.; Deckert, V. Tip-Enhanced Raman Scattering (TERS) of Oxidised Glutathione on an Ultraflat Gold Nanoplate. *Phys. Chem. Chem. Phys.* **2009**, *11*, 7360−7362.

(159) Zhang, R.; Zhang, Y.; Dong, Z. C.; Jiang, S.; Zhang, C.; Chen, L. G.; Zhang, L.; Liao, Y.; Aizpurua, J.; Luo, Y.; Yang, J. L.; Hou, J. G. Chemical Mapping of a Single Molecule by Plasmon-Enhanced Raman Scattering. *Nature* **2013**, *498*, 82−86.

(160) Liao, M.; Jiang, S.; Hu, C.; Zhang, R.; Kuang, Y.; Zhu, J.; Zhang, Y.; Dong, Z. Tip-Enhanced Raman Spectroscopic Imaging of Individual Carbon Nanotubes with Subnanometer Resolution. *Nano Lett.* **2016**, *16*, 4040−4046.

(161) Trautmann, S.; Aizpurua, A.; Götz, I.; Undisz, A.; Dellith, J.; Schneidewind, H.; Rettenmayr, M.; Deckert, V. A Classical Description of Subnanometer Resolution by Atomic Features in Metallic Structures. *Nanoscale* **2017**, *9*, 391−401.

(162) Yano, T.; Verma, P.; Saito, Y.; Ichimura, T.; Kawata, S. Pressure-Assisted Tip-Enhanced Raman Imaging at a Resolution of a Few Nanometers. *Nat. Photonics* **2009**, *3*, 437−441.

(163) Mino, T.; Saito, Y.; Verma, P. Control of Near-Field Polarizations for Nanoscale Molecular Orientational Imaging. *Appl. Phys. Lett.* **2016**, *109*, 041105.

(164) Verma, P.; Ichimura, T.; Yano, T.; Saito, Y.; Kawata, S. Nano-Imaging Through Tip-Enhanced Raman Spectroscopy: Stepping Beyond the Classical Limits. *Laser Photonics Rev.* **2010**, *4*, 548−561.

(165) Mino, T.; Saito, Y.; Verma, P. Quantitative Analysis of Polarization- Controlled Tip-Enhanced Raman Imaging through the Evaluation of the Tip Dipole. *ACS Nano* **2014**, *8*, 10187−10195.

(166) Fourkas, J. T. Rapid Determination of the Three-Dimensional Orientation of Single Molecules. *Opt. Lett.* **2001**, *26*, 211−213.

(167) Shegai, T.; Brian, B.; Miljkovic, V. D.; Kall, M. Angular Distribution of Surface-Enhanced Raman Scattering from Individual Au Nanoparticle Aggregation. *ACS Nano* **2011**, *5*, 2036−2041.

(168) Böhmer, M.; Enderlein, J. Orientation Imaging of Single Molecules by Wide-Field Epifluorescence Microscopy. *J. Opt. Soc. Am. B* **2003**, *20*, 554−559.

(169) Schuck, P. J.; Bao, W.; Borys, N. J. A Polarizing Situation: Taking an In-Plane Perspective for Next-Generation Near-Field Studies. *Front. Phys.* **2016**, *11*, 117804−117817.

(170) Pettinger, B.; Ren, B.; Picardi, G.; Schuster, R.; Ertl, G. Nanoscale Probing of Adsorbed Species by Tip-Enhanced Raman Spectroscopy. *Phys. Rev. Lett.* **2004**, *92*, 096101.

(171) Hartschuh, A.; Sánchez, E. J.; Xie, X. S.; Novotny, L. High-Resolution Near-Field Raman Microscopy of Single-Walled Carbon Nanotubes. *Phys. Rev. Lett.* **2003**, *90*, 095503−095506.

(172) Yano, T.; Ichimura, T.; Taguchi, A.; Hayazawa, N.; Verma, P.; Inouye, Y.; Kawata, S. Confinement of Enhanced Field Investigated by Tip-Sample Gap Regulation in Tapping-Mode Tip-Enhanced Raman Microscopy. *Appl. Phys. Lett.* **2007**, *91*, 121101.

(173) Bailo, E.; Deckert, V. Tip-Enhanced Raman Scattering. *Chem. Soc. Rev.* **2008**, *37*, 921−930.

(174) Hayazawa, N.; Watanabe, H.; Saito, Y.; Kawata, S. Towards Atomic Site-Selective Sensitivity in Tip-Enhanced Raman Spectroscopy. *J. Chem. Phys.* **2006**, *125*, 244706.

(175) Yano, T.; Inouye, Y.; Kawata, S. Nanoscale Uniaxial Pressure Effect of a Carbon Nanotube Bundle on Tip-Enhanced Near-Field Raman Spectra. *Nano Lett.* **2006**, *6*, 1269−1273.

(176) Okuno, Y.; Saito, Y.; Kawata, S.; Verma, P. Tip-Enhanced Raman Investigation of Extremely Localized Semiconductor-to-Metal Transition of a Carbon Nanotube. *Phys. Rev. Lett.* **2013**, *111*, 216101.

(177) Klingsporn, J. M.; Sonntag, M. D.; Seideman, T.; Van Duyne, R. P. Tip-Enhanced Raman Spectroscopy with Picosecond Pulses. *J. Phys. Chem. Lett.* **2014**, *5*, 106−110.

(178) Hayazawa, N.; Yano, T. A.; Kawata, S. Highly Reproducible Tip-Enhanced Raman Scattering Using an Oxidized and Metallized Silicon Cantilever Tip as a Tool for Everyone. *J. Raman Spectrosc.* **2012**, *43*, 1177−1182.

(179) Wagner, M.; McLeod, A. S.; Maddox, S. J.; Fei, Z.; Liu, M.; Averitt, R. D.; Fogler, M. M.; Bank, S. R.; Keilmann, F.; Basov, D. N. Ultrafast Dynamics of Surface Plasmons in InAs by Time-Resolved Infrared Nanospectroscopy. *Nano Lett.* **2014**, *14*, 4529−4534.

(180) Ni, G. X.; Wang, L.; Goldflam, M. D.; Wagner, M.; Fei, Z.; McLeod, A. S.; Liu, M. K.; Keilmann, F.; Özyilmaz, B.; Castro Neto, A. H.; Hone, J.; Fogler, M. M.; Basov, D. N. Ultrafast Optical Switching of Infrared Plasmon Polaritons in High-Mobility Graphene. *Nat. Photonics* **2016**, *10*, 244−247.

DOI: 10.1021/acs.chemrev.6b00821
Chem. Rev. 2017, 117, 6447−6466